Extreme precipitating events in satellite and rain-gauge products over the Sahel

Sidiki Sanogo, Philippe Peyrillé, Romain Roehrig, Françoise Guichard, Ousmane Ouedraogo

To cite this version:

Sidiki Sanogo, Philippe Peyrillé, Romain Roehrig, Françoise Guichard, Ousmane Ouedraogo. Extreme precipitating events in satellite and rain-gauge products over the Sahel. Journal of Climate, 2022, 35 (6), pp.1915-1938. 10.1175/JCLI-D-21-0390.1 . hal-03976472

Extreme precipitating events in satellite and rain-gauge products over the Sahel

Sidiki Sanogo,[a] Philippe Peyrillé,[a] Romain Roehrig,[a] Françoise Guichard,[a] Ousmane Ouedraogo,[b]

[a]CNRM, Université de Toulouse, Météo France, CNRS, Toulouse, France

[b]Agence Nationale de la Météorologie (ANAM), Ouagadougou, Burkina Faso

Corresponding author: Sidiki Sanogo, sidiki.sanogo@meteo.fr

ABSTRACT

Over the recent decades, Extreme Precipitation Events (EPE) have become more frequent over the Sahel. Their properties, however, have so far received little attention. In this study the spatial distribution, intensity, seasonality and interannual variability of EPEs are examined, using both a reference dataset, based on a high-density rain-gauge network over Burkina Faso and 24 precipitation gridded datasets. The gridded datasets are evaluated in depth over Burkina Faso while their commonalities are used to document the EPE properties over the Sahel. EPEs are defined as the occurrence of daily-accumulated precipitation exceeding the all-day 99th percentile over a 1°x1° pixel. Over Burkina Faso, this percentile ranges between 21 and 33 mm day^{-1}. The reference dataset show that EPEs occur in phase with the West African monsoon annual cycle, more frequently during the monsoon core season and during wet years. These results are consistent among the gridded datasets over Burkina Faso but also over the wider Sahel.

The gridded datasets exhibit a wide diversity of skills when compared to the Burkinabe reference. The Global Precipitation Climatology Centre Full Data Daily version 1 (GPCC-FDDv1) and the Global Satellite Mapping of Precipitation gauge Reanalysis version 6.0 (GSMaP-gauge-RNL v6.0) are the only products that properly reproduce all of the EPE features examined in this work. The datasets using a combination of microwave and infrared measurements are prone to overestimate the EPE intensity, while infrared-only products generally underestimate it. Their calibrated versions perform than their uncalibrated (near-real-time) versions. This study finally emphasizes that the lack of rain-gauge data availability over the whole Sahel strongly impedes our ability to gain insights in EPE properties.

1. Introduction

The Sahel is a semi-arid region in West Africa where Mesoscale Convective Systems (MCS) provide most of the rainfall (e.g., Laurent et al. 1998, Mathon et al. 2002). The most intense of them are associated with Extreme Precipitating Events (EPE), which frequently results in flash floods with severe socio-economic damages (Baldassarre et al. 2010; Descroix et al. 2018).

During the last decades, the frequency of occurrence of the most intense MCSs has tripled (Taylor et al. 2017). The EPE frequency of occurrence has also increased and now exceeds that observed during the wet decades of the 1950s and 1960s (Panthou et al. 2014). In the future, their frequency of occurrence is likely to increase (Berthou et al. 2019, Donat et al. 2019), consistently with the intensification of the hydrological cycle induced by global warming (Giorgi et al. 2011).

From a climatological perspective, EPEs roughly contribute to 10-20% of the total annual rainfall over the Sahel (e.g., Panthou et al. 2014, Ta et al. 2016). Their interannual variability is strongly coupled to the interannual variability of total annual rainfall (Diakhaté et al. 2019). Few studies analyzed so far the processes at play in these Sahelian EPEs. The few of them (Lafore et al. 2017, Engel et al. 2017, Beucher et al. 2019), based on two specific EPE case studies emphasize the key role of synoptic-to-intraseasonal timescales in their occurrence.

The EPE properties significantly depend on the definition used for their detection. For instance using the 95th wet-day percentile, Diakhaté et al. (2019) study events leading to more than 20 mm day^{-1}. This intensity is consistent with the heavy precipitating events (return frequency less than 10 times per year) studied in Panthou et al. (2014). In contrast, Panthou et al. (2014) define an EPE as an event with a return frequency less than 2.5 times per year leading to EPE rain rates above 40 mm day^{-1}. In fact the use of different definition of EPEs hampers comparisons of the findings of many studies (e.g., Alexander et al. 2019). For this reason the Expert Team on Climate Change Detection and Indices defined ten indices for the analysis of precipitation, among which the wet-day 99th percentile (wet-day indicating days with rainfall greater than 1 mm day^{-1}) is intended to detect the extremely wet days (Zhang et al. 2011). However Schär et al. (2016) emphasize that the wet-day percentile approach hides a strong sensitivity to the wet-day frequency of occurrence, which can make analyses more complex, especially in the context of intercomparisons. This issue is probably even more critical in West Africa as current rainfall products strongly differ with respect to this wet-day frequency (Cassé et al. 2015, Sylla et al. 2013).

For a robust statistical documentation of EPEs, long time series of reliable precipitation estimates are needed. A rain-gauge network offers the appropriate temporal sampling, but the scarcity of the Sahel network (Taupin et al. 1998) often limits its use for regional analyses of EPEs. At the scale of a 1°x1° Sahelian pixel, Gosset al. (2018) show that at least five stations are needed to make a relevant rainfall estimate. The low density of the rain-gauge network over the Sahel and the reduced access to associated data make it difficult to achieve this requirement. This significantly impedes the study of EPE over the Sahel.

Precipitation estimates based on satellite measurements offer a unique alternative with higher spatial coverage compared to rain-gauge data. However, these estimates often exhibit significant biases (e.g., Beck et al. 2017; Gosset al. 2013; Huffman et al. 1997; Nicholson et al. 2003a,b; Roca et al. 2010; Satgé et al. 2020), from daily precipitation rates to seasonally-cumulated rainfall amounts. Masunaga et al. (2019), Sun et al. (2018) and Herold et al. (2017) show that such products also have uncertainties on the EPE intensity worldwide, especially in regions with sparse rain-gauge networks. Over the Sahel, the analysis of the well-documented EPE that occurred on September 1, 2009 in Ouagadougou, Burkina Faso, indicates that a local station recorded 261.3 mm day^{-1} (Lafore et al.2017, Engel et al. 2017) while, in the 0.25°x0.25° pixel containing this station, TMPA-3B42 (see Tables 1, 2 for the acronym definition of each product used in this paper) and PERSIANN-CDR retrieved 70 mm day^{-1} and 40 mm day^{-1} respectively (Engel et al. 2017). This example points out the difficulty to quantitatively observe EPEs.

In the literature, several studies attempt to document the EPE statistical properties by intercomparing or evaluating gridded rainfall products over West Africa. For instance Odoulami et Akinsanola (2018), Crétat et al. (2015) and Sylla et al. (2013) find important differences between GPCP, TMPA-3B42 and RFE for the wet-day 95th percentile values and the associated spatial pattern over West Africa. Cassé et al. (2015) and Gosset et al. (2013) show that precipitation dataset (P-dataset hereafter) uncertainties are large with respect to the EPE contribution to total annual rainfall. The careful product evaluations conducted by Gosset et al. (2013, 2018) and Roca et al. (2010) at the well-instrumented sites of Niamey, Dakar and Ouémé also report large uncertainties for the whole distribution of daily rainfall. However, it should be noted that most of these studies intercompared a limited number of datasets among the wide diversity that is currently available. Most of these studies also focused only on one to three distant pixels. These limitations, together with the fact that the P-datasets are often considered at their native spatial resolution, thus different, spatial resolution, make the conclusions difficult to generalize and limit the possibility to identify robustly the EPE properties across the Sahel.

Our objective is twofold: (i) provide a systematic evaluation of the EPE climatological properties as captured by 24 gridded P-datasets against a reference dataset based on a dense network over Burkina Faso (142 rain-gauge) and (ii) document the EPE climatological properties over the Sahel by considering the commonalities among the P-datasets, while emphasizing areas where large inconsistencies prevent to draw robust conclusions. We use the all-day percentile approach at the daily temporal scale and the 1°x1° spatial scale (results based on wet-day percentiles are only briefly discussed). The longest common period among P-datasets (2001-2013) is considered to quantitatively define EPEs and thereby provide a fair basis for P-dataset comparison. Longer periods are used when documenting the EPE interannual variability.

The paper is structured as follows. Section 2 details the P-datasets used in the present study and describes the methodology used to analyze EPEs over the Sahel. Section 3 characterizes rainfall distribution and EPEs over Burkina Faso. Section 4 accounts for the spatial and temporal variability of EPEs. Section 5 discusses the sensitivity of the results to the use of the wet-day percentile definition and the performance of the near-real-time products. Section 6 summarizes our main findings.

2. Data and methods

a. Data

We considered the daily 1°x1° mean areal rainfall to define and study EPEs. This scale stands as a minimum resolution for which P-datasets show the largest agreement for extreme and heavy rainfall events (Herold et al. 2017). A dense rain-gauge network over Burkina Faso is used to build a reference dataset and evaluate 24 gridded P-datasets at this scale. These datasets are issued from the Frequent Rainfall Observations on GridS (FROGS) database (Roca et al.2019) except for MSWEP and RFE. Note that daily-accumulated rainfall a priori refers to as rainfall accumulated from 00:00 UTC to 00:00 UTC the following day (standard of the FROGS datasets), while the reference dataset provides rainfall accumulated on a 06:00 UTC – 06:00 UTC basis. Sub-daily P-datasets (TMPA 3B42 v7 and RFE v2) indicate that the induced mismatch is weak, mostly below 1-2 mm day^{-1} for the rainfall 99th percentile (not shown), well below the inter-product spread. It therefore does not impact our results.

1) REFERENCE P-DATASET

Our reference dataset is built from 142 rain-gauge stations covering most of Burkina Faso (Fig. 1a). They provide daily-accumulated precipitation summaries over the period 1995-2016. This dense rain-gauge network includes the 10 Burkinabe synoptic stations of the Global Telecommunication System (GTS). The network exhibits often more than 5 stations within each 1°x1° pixel. The densest pixel (3E on Fig. 1a) encompasses 15 stations. Following Gosset et al. (2018) we only considered 1°x1° pixels that contain at least 5 stations, and thus ensure a proper evaluation of precipitation characteristics at this scale.

2) GRIDDED DATASETS BASED ON RAIN-GAUGE OBSERVATIONS ONLY

The gridded rain-gauge-based P-datasets used here are GPCC-FDDv2018, GPCC-FDDv1, REGEN, REGEN40YR and CPC (Table 2). Over Africa the main differences between these datasets originate from the rain-gauge networks and interpolation schemes on which they rely. The GPCC rain-gauge network is used as a basis for all these products except CPC, which uses a less dense network (Contractor et al. 2020, Sun et al. 2018). In addition to the GPCC network, REGEN and REGEN40YR include all stations from the Global Historical Climate Network (GHCN-Daily), with a restriction to stations that report a minimum of 40 years of data for REGEN40YR (Contractor et al. 2020). Over Burkina Faso these networks include at most 2 stations per pixel and thus weakly overlap our reference (Fig. 1, see also Fig. S1 in the supplemental material).

GPCC-FDDv2018, GPCC-FDDv1, REGEN and REGEN40YR are respectively retrieved by interpolating the ratios between daily and monthly totals and retrieving the absolute rainfall values by superimposing gridded monthly total fields on the interpolated ratios (Contractor et al. 2020, Beck et al. 2013, Ziese et al. 2018). GPCC-FDDv1, REGEN and REGEN40YR use ordinary block kriging (Contractor et al. 2020, Beck et al. 2013), while GPCC-FDDv2018 uses a modified inverse distance weighting scheme, referred to as SPHEREMAP (Ziese et al. 2018). CPC is based on the optimal interpolation technique described in Chen et al. (2008).

3) GRIDDED DATASETS BASED ON SATELLITE MEASUREMENTS

(i) Infrared-based P-datasets

We evaluated five precipitation datasets, which use the Geosynchronous Earth Orbit InfraRed (GEO-IR) data as a main input, generally together with a rain-gauge-based calibration procedure: ARC, TAMSAT, CHIRPS, CHIRP and PERSIANN-CDR (Table 2). ARC ingests GEO-IR data linearly through a maximum likelihood method. The final estimates are bias-corrected using the methodology of Reynolds (1988) and the GTS daily precipitation data (Novella and Tiaw, 2013). TAMSAT develops a local calibration of satellite precipitation estimates with GEO-IR data using historical rain-gauge data (Maidment et al. 2017). CHIRP uses TMPA-3B42 (Funk et al. 2015) as a training dataset to calibrate its GEO-IR-based algorithm. CHIRP is primarily produced at the pentadal timescale and further disaggregated using the Coupled Forecast System Reanalysis Version 2 daily data which is corrected using the Climate Hazards Center's Precipitation Climatology (CHPclim) (Funk et al. 2015). CHIRPS is derived from CHIRP through bias-correction at the monthly and pentadal time scales using the GTS, GHCN monthly and daily, and the Global Summary Of the Day databases. PERSIANN-CDR is obtained by applying the Precipitation Estimation from Remotely Sensed Information using Artificial Neural Networks (PERSIANN) algorithm to the historical archive of GEO-IR observations. PERSIANN-CDR is then bias corrected with the monthly GPCP dataset (version 2.2).

(ii) P-datasets incorporating microwave measurements

Our study includes the microwave (MW) P-datasets TMPA-3B42, IMERG-FC, GPCP-CDR, CMORPH-CRT, GSMaP-gauge-RNL and RFE. A few near-real-time products are also considered: TMPA-3B42RT, IMERG-EU, IMERG-LU, CMORPH-Raw, GSMaP-gauge-NRT and GSMaP-no-gauge-NRT (Table 2). This category of precipitation datasets takes advantage of the high temporal resolution of the GEO-IR observations and the high accuracy of rainfall estimate from MW sensors onboard Low-Earth-Orbit satellites. Their building process consists of three main steps. (i) The precipitation estimates are retrieved for each single MW sensors, based on their own algorithm and calibration process. (ii) Then, the various MW estimates are combined, together with the IR estimates. During this step, TMPA-3B42 and GPCP-CDR use a probability matching approach (Huffman et al. 2001, 2007). CMORPH-CRT follows the CPC morphing technique algorithm (Xie et al. 2017). GSMaP products use the morphing technique together with a Kalman filter (Kubota et al. 2007, see also GSMaP Technical Documentation – GTDS2014). In the retrieving process, GSMaP-gauge-RNL uses the atmospheric conditions from the Japanese 55-year Reanalysis (JRA-55) while GSMaP-gauge-NRT and GSMaP-no-gauge-NRT use the Japan Meteorological Agency forecast data as atmospheric information (GTDS2014). IMERG-FC uses CPC morphing-Kalman filter and the PERSIANN-Cloud Classification System (PERSIANN-CCS, Huffman et al. 2020). RFE combines IR and MW estimates linearly through a maximum likelihood method (Novella et Thiaw 2013). (iii) The final step consists in a bias correction procedure. GPCP-CDR, TMPA-3B42 and IMERG-FC are bias-corrected at the monthly time scale using the GPCC monthly dataset (Huffman et al. 1997, 2001, 2007, 2020). CMORPH-CRT and GSMaP-gauge-RNL are bias-corrected at the daily time scale using CPC through a probability matching approach (Kubota et al. 2007; Xie et al. 2017).

Note that the GSMaP-gauge-NRT does not directly ingest the rain-gauge data but uses the error parameters computed from GSMaP-gauge (not analyzed here) to adjust GSMaP-no-gauge-NRT (GTDS2014). RFE uses the same approach as ARC for bias correction (Novella et Thiaw 2013).

MSWEP and SM2RAIN-CI follow a different strategy for including MW information. MSWEP federates CPC daily data, GPCC monthly rainfall at 2.5°, as well as model reanalysis (ERA-Interim and JRA-55) and the near-real time MW-based products TMPA-3B42-RT, GSMaP-MVK and CMORPH (Beck et al. 2017). SM2RAIN-CI is based on the analysis of the soil water balance with as an input the active and passive ESA CCI Soil Moisture (SM) products. It then uses GPCC-FDDv1 for calibration at the pentadal time scale (Ciabatta et al. 2018).

b. Methods

1) SPATIAL REGRIDDING

All products in the FROGS database are provided at a 1°x1° / daily resolution after a conservatively regridding based on a simple arithmetic mean applied to the products having a finer spatial resolution (Roca et al. 2019). RFE, MSWEP are interpolated to the 1°x1° resolution using the second-order conservative scheme of Jones (1999).

The daily precipitation reference dataset over Burkina Faso is derived as the arithmetic mean of the rainfall records from all the stations encompassed within each of the 1°x1° pixels.

2) EPE DEFINITION AND TIME PERIODS USED

EPEs are determined for all datasets as days with rainfall exceeding the 99th all-day percentile. The use of a percentile definition rather than a fixed threshold approach allows for a fair comparison between different products that might have differences in their distribution of precipitation. The all-day percentile definition is used here to ease the comparison between the different P-datasets as they exhibit a large range of wet-day frequency of occurrence over the Sahel. The sensitivity of the results to the use of a wet-day percentile definition is nevertheless discussed in Section 5. The sensitivity to the percentile rank used to define EPEs is weak and is presented in the supplemental material.

The time period used to estimate statistical properties of the rainfall distribution, and in particular EPE characteristics, is critical. For the sake of consistency, the longest common period among P-datasets (2001-2013) to compute the percentile used to detect EPEs. The P-dataset evaluation is conducted over this common period (their robustness to the chosen period was tested – not shown), while an extended period is also considered for the analysis of the EPE interannual variability (longest common period between the reference and each P-dataset – see Tables 1, 2).

3) SIGNIFICANCE OF THE RESULTS

Estimates of high percentile are sensitive to the sample size. Therefore, the uncertainty of these estimates is evaluated using a non-parametric bootstrap approach (Efron et Tibshirani 1994). Confidence intervals are determined as follows: (i) a set of 1000 samples of the same size as the original sample is constructed by sampling the original dataset elements with replacement, (ii) for each of the 1000 samples, the percentile of interest is computed. The percentile distribution based on these 1000 estimates provides a confidence interval at the 95% significance level.

For the specific case of the reference dataset, uncertainties also arise because of the relatively small number of stations within each 1°x1° pixel (e.g., Gosset et al. 2018; Lebel et Amani, 1999). For a given pixel, a first (spatial) bootstrap process is performed to generate 500 new time series of daily precipitation, based for each day on the station records available for this pixel. For each of these time series, a second bootstrap process of size 1000 is applied to estimate a distribution of the targeted percentile. The final confidence intervals used for the reference dataset thus includes the uncertainties linked to both the sampling size and the number of stations within a 1°x1° pixel.

3. EPE intensity over Burkina Faso

a. EPE distribution

As stated in Section 2.b.2, EPEs are here defined based on the 99th all-day percentile over the period 2001-2013. Over Burkina Faso, the 99th percentile ranges from 21 to 33 mm day^{-1} at the 1°x1° pixel scale (Fig. 1b). At the local (station) scale, it often translates into daily rainfall rate in the 40-80 mm day^{-1} range (not shown). Such amounts can lead to significant hydrological impacts and floods (Tarhule 2004). The scatter plot of Figure 2b compares for each of the 15 pixels covering Burkina Faso the 99th percentile of each P-dataset to those estimated with our rain-gauge reference. Note that near-real-time P-datasets are considered in Section 5.b and thus are not displayed on Figures 2-13, for the sake of clarity, but also because of their different nature and underlying objectives. The inter-product spread is large, ranging from 15 to 40 mm day^{-1} (46 % to 118 % of the reference intensity). The precipitation datasets behave consistently across the 15 pixels.

Figure 2a positions the EPE intensity of the densest pixel (3E on Fig. 1) with respect to the full daily precipitation distribution, based on the quantile-quantile relationship between each P-dataset and the reference. It highlights that the inter-product spread is consistent from approximately the 92.5th percentile and increases with the chosen percentile: the spread reaches around 20 mm day^{-1} for the 98th percentile (to be compared to ~20 mm day^{-1} for the reference), and more than 35 mm day^{-1} for the 99.5th percentile (~30 mm day^{-1} for the reference). A large fraction of the spread is driven by two datasets, namely SM2RAIN-CI and

TAMSAT, which dramatically underestimate the highest percentiles. In contrast, the other datasets are rather packed together, between percentile values consistent with those of the reference and significantly overestimated percentile values.

b. Best subset of P-datasets

Figure 2c synthesizes the P-dataset behavior for pixel 3E, accounting for the sampling uncertainty (Section 2.b.3). First, the 99th percentile reference uncertainty is about +/- 2 mm day^{-1}, and its bootstrap median value about 26 mm day^{-1}, close to the raw estimate. Three groups of P-datasets emerge for that pixel:

(i) A first group provides estimates consistent with the reference and includes the infrared-based precipitation dataset ARC, the MW-based dataset RFE and the rain-gauge precipitation datasets REGEN, REGEN40YR, GPCC-FFDv1.

(ii) The second group overestimates the 99th percentile and includes most of the MW+IR datasets (TMPA-3B42, IMERG-FC, GPCP-CDR, GSMaP-gauge-RNL, CMORPH-CRT) and the rain-gauge products GPCC-FDDv2018 and CPC.

(iii) Finally, the third group significantly underestimates the EPE intensity and consists of SM2RAIN-CI, TAMSAT, PERSIANN-CDR and CHIRPS.

To further examine the skill of the P-datasets at the scale of the 15 pixels covering Burkina Faso, we introduce the implausibility measure used in the framework of history matching (e.g., Craig et al. 1996, Bower et al. 2010). To our knowledge, this is the first time it is applied in such an evaluation context. The rationale behind is not to identify the best dataset in the sense of a given deterministic score, but to identify the datasets that are consistent with the reference, given the estimated uncertainties. The approach acknowledges that there are uncertainties, and that they need to be accounted for both in the skill measure and in the way to interpret it. The implausibility measure is close to the natural Euclidean distance except it introduces the variance of the considered uncertainties, following the Mahalanobis distance (Mahalanobis, 1936), assuming a diagonal covariance matrix (i.e. no error correlation between the 15 pixels). It reads (see also Salter et al. 2019):

$$I_q^d = \sqrt{\frac{1}{p}\sum_{k=1}^{p}\frac{\left(\overline{P_{q,k}^{d}} - \overline{P_{q,k}^{ref}}\right)^2}{\left(\sigma_{q,k}^{d}\right)^2 + \left(\sigma_{q,k}^{ref}\right)^2 + \delta_q^2}}$$

where the $p=15$ is the number of pixels, $P_{q,k}^{d}$the q^{th} percentile of the dataset d for the pixel k, $P_{q,k}^{ref}$ that of the reference dataset, $\sigma_{q,k}^{d}$ the bootstrap estimated standard deviation of $P_{q,k}^{d}$ and $\sigma_{q,k}^{ref}$ that of the reference. The bootstrap quantile estimates approximately behave as a Gaussian distribution (not shown). The overbar indicates the expected value of the variable, based on the bootstrap distribution. Among the sources of uncertainty, the structural error δ_q of the P-datasets (or discrepancy between the real world and the datasets representing it) is also introduced. It is a priori unknown and is interpreted here as a tolerance to error (e.g., Williamson et al., 2015). It is parameterized here as being proportional to $\overline{P_{q,k}^{ref}}$. This tolerance level is clearly user-dependent and should be adjusted for each application. We arbitrarily choose a 5% tolerance to error (1-2 mm day^{-1} over Burkina Faso), meaning that a 5% error on a given percentile would still correspond, in our opinion, to a skillful P-dataset to study EPEs over Burkina Faso, and possibly over the Sahel regions with similar precipitation regimes. Further assuming that the pixel distributions are independent, $p\left(I_q^d\right)^2$ follows a χ-square distribution with $p=15$ degrees of freedom (e.g., Bower et al., 2010, Salter et al., 2019). Given a confidence level (95% and 99% on Figure 2d), the P-dataset that provides percentile estimates incompatible with the reference can be discriminated from, those that are consistent with the reference dataset, given the estimated uncertainties. Figure 2d thus indicates that REGEN, GPCC-FDDv1, GSMaP-gauge-RNL, IMERG-FC, CMORPH-CRT are consistent with the reference over the 15 pixels covering Burkina Faso, givent a 5% tolerance error. Similar results are obtained with the 98th and 99.5th percentiles (Fig. S3). This subset of P-datasets is further used in the following to document EPE intensities over the whole Sahel in particular to investigate whether they exhibit a larger agreement apart from Burkina Faso.

4. EPE spatial and temporal variability

a. Spatial distribution

Figure 3 shows the spatial distribution of the 99th percentile as proposed by each P-dataset. All datasets exhibit a first-order meridional gradient over West Africa, despite a large spread along the Guinea Coast, and over Eastern and Central Africa. In contrast, there is a wider diversity in the zonal variations of the 99th percentile. The large spread in the EPE intensity shown here is consistent with results obtained in previous studies (e.g., Crétat et al. 2013, Sylla et al. 2013, Herold et al. 2017, Masunaga et al. 2019, Odoulami et Akinsanola 2018, Sun et al. 2018).

A few consistencies are worthwhile to be noted:

(i) REGEN, REGEN40YR and GPCC-FDDv1 provide similar distributions (Figs. 3,h,i,j), except over Nigeria and Central Africa (e.g., Cameroon, Republic of Central Africa and Congo). This agreement is likely expected since the three datasets uses similar rain-gauge networks and similar interpolation algorithms. In contrast, GPCC-FDDv2018 (Fig. 3a), which uses similar input data but a different interpolation algorithm, is very different from GPCC-FDDv1. As GPCC-FDDv1 is closest to our reference over Burkina Faso, this questions the use of GPCC-FDDv2018 interpolation algorithm, at least with respect to EPE intensity.

(ii) TMPA-3B42 and its successor IMERG-FC are remarkably similar across the region (Figs. 3d,e), although their near real-time counterparts exhibit large differences (Fig. 15) indicating the rain-gauge bias correction strongly impacts the final precipitation estimates.

(iii) CMORPH-CRT, GSMaP-gauge-RNL and GPCP-CDR exhibit a 99th percentile maximum in the 10°N-15°N band, over Mali, Burkina Faso and Nigeria (weaker agreement for the latter though). It remains unclear whether this structure traces back to intrinsic properties of the P-datasets algorithms, or to physical differences between convective systems between the Sahel and the Guinean Coast, or different rain-gauge networks used for bias-correction.

(iv) MSWEP and SM2RAIN-CI use very different strategies for retrieving precipitation. In both cases, they provide generally weak values of the 99th percentile. For MSWEP, this may be related to the use of reanalysis precipitation data, known to underestimate the occurrence of heavy rainfall events and overestimate that of wet days (daily rainfall > 1 mm day^{-1}, e.g., Diaconescu et al. 2014). Given the previous results over Burkina Faso (Fig. 2), the soil-moisture-based approach can be disqualified for the analysis of rainfall extremes. TAMSAT also belongs to the datasets providing weak 99th percentile values over the Sahel, which is consistent with Maidment et al. (2017, see their Fig. 4) and the overall TAMSAT objective to focus more on weak rainfall rate retrievals important for drought monitoring (Maidment et al. 2017).

The spatial distribution of the 99th percentile and its properties among the P-datasets is further assessed on Figure 4 by grouping them according to their main input data, namely rain-gauge only (Figs. 4a,e,i), IR only (Figs. 4c,g,k) and MW-based (Figs. 4b,f,j). Note that SM2RAIN-CI is excluded from each of these three groups, while MSWEP is considered in the full ensemble used on Figures 4d,g,l. Consistently with Figures 2a,b, IR products provide lower EPE intensity. MW-based and rain-gauge-based products are more similar, except over highland and Central Africa regions (Figs. 4a-c). The latter regions correspond to the locations where the dataset spread is the largest (Figs. 4e-g).

To quantify the level of agreement between the P-datasets, we introduce the following coefficient of agreement $C_A = \left(1 - \frac{\sigma}{\mu}\right) * 100$, where μ and σ are the P-dataset ensemble mean and standard deviation, respectively. A value of 100% indicates the highest level of agreement between the datasets. Rain-gauge-only products exhibit a weaker agreement over West Africa than IR-only and MW-based products, in particular over the Eastern and Northern Sahel and Central Africa (Figs. 4 i,j,k). This may emphasize the sparse rain-gauge network over these regions, which also varies from one dataset to another. In contrast satellite products intrinsically encompass more spatial homogeneity. In particular, the MW-based P-datasets impressively agree well over all the regions (often above 90%), except along the Sahara margins and the Guinean Highlands. Such a consistency is also noted in their precipitation distribution shown on Fig. 2.

Similar diagnostics for the best subset identified in Section 3.b over Burkina Faso are shown on Figure 5. This group includes REGEN, GPCC-FDDv1, IMERG-FC, CMORPH-CRT, and GSMaP-gauge-RNL. These P-datasets reasonably agree over a wide area south of 15°N, often exceeding a level of 80% (Fig. 5c). Notable exceptions are the Guinean Highlands, northern Niger and Sudan, similarly to the groups previously considered (Fig. 4). For the regions of high agreement within this best subset, in particular over the Central and Western Sahel, we may consider that they provide a reasonable description of the EPE spatial distribution. Over the Sahel, the 99th percentile values transition from 24 mm day^{-1} near 15°N to less than 12 mm day^{-1} near 18°N. Over the Guinean and Soudanian regions, the subset-mean 99th percentile values range between 24 and 33 mm day^{-1} with a standard deviation less than 4 mm day^{-1} (Fig. 5a, b).

The latitudinal dependence of the EPE intensity (average of the EPE daily rain rates) is emphasized on Figure 6, together with that of mean annual rainfall. We consider zonal averages between 5°W and 2°E, which spans both the area of the Burkina Faso reference dataset, and the area of highest level of agreement among all P-dataset (Fig. 4).

All datasets consistently capture the south-to-north decrease of the mean annual rainfall, from about 1150 mm year^{-1} near 10°N to about 150 mm year^{-1} near 18°N (Fig. 6a). This corresponds to a decreasing rate of 125 mm year^{-1} per degree of latitude (see also Fink et al. 2017). In contrast, the spread is much larger in the Guinean and Soudanian regions (5.5°N to 10°N), where mean annual rainfall ranges from 1100 mm year^{-1} (CMORPH-CRT) to 1300 mm year^{-1} (GPCC-FDDv2018) near 8°N. The ensemble mean (red dots) well agrees with the reference data over Burkina Faso (thick black line), and suggests decreasing rate of 45 mm year^{-1} per degree of latitude from 5.5°N to 10°N.

The EPE intensity meridional structure is broadly similar in shape to that of mean annual rainfall (Figs. 6a, b). However, the inter-product spread in the EPE mean intensity is large, especially compared to that of mean annual rainfall. It emphasizes how bias correction (or the direct input of rain-gauge data) efficiently constrains the mean annual rainfall, while having weaker influence on the details of the precipitation distribution. The inter-product spread is larger between 6°N and 12°N, with many datasets showing a plateau in the EPE intensity. A few datasets exhibit a maximum between 12°N and 15°N (e.g., GPCP-CDR), consistent with Fig. 3. Over the Sahel (12°N to 18°N), the decreasing rate of EPE intensity is slightly higher in GPCC-FDDv2018, GPCP-CDR, CPC, TMPA-3B42, CMORPH-CRT and IMERG-FC (3-4 mm day^{-1} per degree of latitude) than in the other datasets (1.25-3 mm day^{-1}

per degree of latitude). It can be noticed that the products consistently behave over both Burkina Faso and the whole West Africa: the products which overestimate the EPE intensity over Burkina Faso also provide the highest EPE intensities over the whole West Africa, and vice-versa. The ensemble mean (red dots) suggests an EPE intensity around 40 mm day^{-1} between 6°N and 12°N, and a decrease of 3 mm day^{-1} per degree of latitude from 12°N to 18°N. Over Burkina Faso this EPE intensity is about 37 mm day^{-1} in the reference product. The best subset identified in Section 3.b (blue dots) indicates a slightly higher EPE intensity (~40 mm day^{-1}), thereby emphasizing the uncertainty of the reference value.

b. Seasonality

The mean annual cycle of rainfall and EPE occurrence over Burkina Faso is shown on Figure 7a, based on the reference dataset. The annual cycle of rainfall is typical of a monsoon regime with more rain (above 4 mm day^{-1}) from June to September, and much less or no rain at all during the rest of the year (cyan bars). The EPE occurrence annual cycle (grey bars) is strongly coupled to that of the mean annual rainfall, with a higher frequency during the core monsoon season (grey bars). This suggests more favorable environments for EPEs during the monsoon season. The EPE frequency peaks in August, with on average about 1 event year^{-1} pixel^{-1} (note that the peak occurs during the last two decades of August – not shown).

Several P-datasets broadly capture the coupling between the monsoon and EPE occurrence annual cycles (Figs. 7b-r). REGEN, GPCC-FDDv1, CMORPH-CRT, GSMaP-gauge-RNL, GPCP-CDR, TMPA-3B42 agree the most with the reference, followed by GPCC-FDDv2018, RFE, ARC, IMERG-FC. A few datasets such as CHIRPS and PERSIANN-CDR tend to overestimate the EPE frequency of occurrence in August and the months around, while underestimating it during the beginning and end of the monsoon season. A few other datasets slightly shift the EPE annual cycle towards the early monsoon months (e.g., ARC, RFE), with SM2RAIN-CI and TAMSAT being strong outliers in this respect. Except for TAMSAT, there is no clear relationship between the biases in the EPE frequency of occurrence annual cycle and those in the rainfall annual cycle (compare Figs. 7 and S16).

Figure 8 extends the previous results to the 5°W-2°E West African transect, considering the time-latitude evolution of monthly precipitation (solid contours) compared to that of EPE occurrence (shading) and intensity (dashed contours). Precipitation datasets consistently capture the rainfall annual cycle and its latitudinal dependence. In March, the rainfall band is located over the Guinean coast. It reaches its maximum intensity in June and then abruptly jumps to the North over the Sahel (Sultan and Janicot, 2000, 2003). There, the monsoon peak occurs in August, at the same time the rainfall band reaches its northernmost latitude. In contrast, very low convective activity occurs on the Guinean coast. In September, the rainfall band gradually withdraws southward, towards the Guinean coast.

The coupling between the monsoon annual cycle and the EPE frequency occurrence is observed over the whole Sahel and is broadly consistent among the P-datasets (Fig. 9): EPEs are more frequent and contributes more to the mean rainfall in July-August-September. A similar coupling is also found along the Guinean Coast (not shown).

c. EPE interannual variability

The interannual variability (IAV) of the EPE annual number and contribution to the total annual rainfall over Burkina Faso is shown on Figure 10a-b, together with that of total rainfall (Fig. 10c). The use of the 99th percentile in the EPE definition implies the occurrence of 3.65 events year^{-1} pixel^{-1}, on average. In the reference dataset, the IAV of the EPE frequency ranges between about 2 and 5 events year^{-1} pixel^{-1}. All products approximately agree on the reference dataset interannual variability, but often with a wider range, as in RFE, REGEN40YR and PERSIANN-CDR (from ~1 to ~6.5 events year^{-1} pixel^{-1} – Fig. 10a). For several years (e.g. 1999 and 2014), the inter-product spread often exceed 2 events year^{-1} pixel^{-1}. Despite this spread, a few years are highly consistent among most of the datasets, e.g., 2003 which was particularly favorable to EPE occurrence (~5-6 events year^{-1} pixel^{-1}), and 2011 which in contrast had very few events (~2 events year^{-1} pixel^{-1}). The reference product indicates a mean EPE contribution of 127 mm year^{-1} to the total annual rainfall (about 800 mm year^{-1} thus ~16%). This contribution fluctuates between 70 mm year^{-1} and 180 mm year^{-1} (Fig. 10b). The spread among the P-datasets is high, in terms of both the mean EPE annual rainfall (see also Cassé et al. 2015) and its interannual variability. In particular, the EPE contribution to annual rainfall, and its IAV amplitude is very weak in SM2RAIN-CI and TAMSAT. Note that the IAV of the EPE contribution to annual rainfall is mainly driven by the number of EPEs in a given year rather than the variability in the EPE intensity (correlation above 0.95).

Similar results are found at the regional scale, namely over the Western, Central and Eastern Sahel (Fig. 11): EPE frequency of 2 to 6 events year^{-1} pixel^{-1}, EPE contribution to the mean annual rainfall ranging between 17 and 22% and interannually fluctuating between +/- 50% of its mean value, and concomitance between wet years and EPE occurrence increase. The Western Sahel exhibits the highest inter-product spread, especially for the IAV of annual rainfall and EPE contribution (Fig. 11d,g). The P-datasets also consistently provide a decrease of mean annual rainfall and EPE contribution from the Western to the Central and the Eastern Sahel.

Figures 12a,b,c quantitatively evaluate the precipitation dataset skill to capture the IAV of EPE number and rainfall. Most products (notable exceptions are TAMSAT and SM2RAIN-CI) exhibit correlation with the reference dataset higher than 0.8 for both the IAV of EPE annual number and the EPE contribution to annual rainfall (black and red symbols on Figure 12c), either over the relatively short period 2001-2013 (red and black dots) or over the largest period of each dataset common with that of the reference (open red and black squares). For the EPE annual number, GPCC-FDDv1 exhibits the highest correlation (0.95 over the period 2001-2013), and is closely followed by GPCC-FDDv2018, CMORPH-CRT, GSMaP-gauge-NRL and MSWEP (correlations above 0.9).

The root mean square error (RMSE) is used to quantify the P-dataset errors on EPE annual number and rainfall (Figs. 12a, b). In terms of annual EPE number (Fig. 10a), and over the period 2001-2013 (full dots), GPCC-FDDv2018, TMPA-3B42, CPC, CMORPH-CRT, GSMaP-gauge-RNL, GPCC-FDDv1, ARC and MSWEP display the highest consistency with the reference, with a mean error less than 0.65 events year^{-1} pixel^{-1} (to be compared with a mean occurrence of 3.6 events year^{-1} pixel^{-1} and with an IAV of 1 events year^{-1} pixel^{-1}). The error is slightly larger for GPCP-CDR, IMERG-FC, RFE, CHIRPS, PERSIANN-CDR (above 0.8 events year^{-1} pixel^{-1}). REGEN, REGEN40YR, TAMSAT present the lowest skill for the IAV amplitude of the EPE annual number (error larger than 0.8 event year^{-1} pixel^{-1}). Regarding the EPE annual rainfall (Fig. 12b), GSMaP-gauge-RNL, GPCC-FDDv1, ARC, CHIRPS and PERSIANN-CDR exhibit the highest skill (error less than 30 mm year^{-1} thus ~23 % of the reference mean EPE annual rainfall) followed by GPCP-CDR, CPC, CMOPRH-CRT, IMERG-FC, REGEN, REGEN40YR, RFE and MSWEP (less than 45mm year^{-1}). GPCC-FDDv2018, TMPA-3B42, TAMSAT and SM2RAIN-CI perform the worst, with RMSE higher than 45 mm year^{-1} (up to 70 mm year^{-1} for SM2RAIN-CI). Note that the evaluation period only marginally impacts the computed skills (compare full dots with open squares).

As a result, GPCC-FDDv1, CMORPH-CRT and GSMaP-gauge-NRL capture both EPE mean properties and IAV, thus appearing as the most relevant datasets to study EPE over Burkina Faso, and probably over the Sahel. In particular, REGEN and IMERG-FC, which scored well for the EPE intensity (see Section 3.b.), exhibit rather weak performance for the EPE interannual variability.

d. Interannual coupling between EPE and annual rainfall

We emphasized previously the strong coupling between EPE occurrence and the monsoon IAV, as years with a high EPE frequency often correspond to monsoon wet years, and vice versa (see also Diakhaté et al. 2019). Figure 13 further quantifies this relationship for Burkina Faso and the three Sahelian domains: for each dataset, the correlation between the EPE annual number and total annual rainfall is computed (red dots), as well as the correlation between EPE mean annual rainfall and total annual rainfall for all P-datasets (black dots). Over Burkina Faso (Fig. 13a), the strong interannual coupling between EPE and annual rainfall is thus confirmed, as the reference dataset indicates correlations above 0.9 for both relationships, and slightly weaker (still above 0.85) when the longest period of the dataset is considered (open squares). Most P-datasets underestimate these relationships. Only GPCC-FDDv2018, CPC, GSMaP-gauge-RNL, GPCC-FDDv1 and REGEN approach similar correlations. In contrast, TAMSAT and SM2RAIN-CI underestimate them the most, providing correlation weaker than 0.75. This coupling is also found significant in most P-datasets over most of the Sahel (Fig. 13c), though slightly weaker and less consistent across P-datasets over the Western and Eastern Sahel (Fig. 13b,d). REGEN40YR stands out from the other datasets, possibly because of a sparser rain-gauge network density. Note that the interannual standard deviation of EPE contribution to total annual rainfall is approximately

34 mm year^{-1}. In contrast, that of total annual rainfall is about 71 mm year^{-1}, meaning that EPEs only account for a small fraction of the rainfall interannual variability over the Sahel.

5. Discussion

a. Wet-day or all-day percentiles?

Many studies use a wet-day percentile approach to define EPE, wet days arbitrarily corresponding to days with rainfall above 1 mm day^{-1}. As discussed in Schär et al. (2016), the use of a wet-day percentile definition requires caution, especially when comparing datasets, as differences may emerge solely because of difference in the wet-day frequency of occurrence. Nevertheless, we analyze the sensitivity of our main results to the use of a wet-day percentile approach instead of considering all-day of a given period.

The spread in the wet-day frequency among P-datasets is first assessed on Figure 14a. It is rather marked near the Coast of Guinea (~90 days year $^{-1}$) and decreases northward (40 days year $^{-1}$ over the Sahel near 15°N). This large spread is consistent with earlier studies over West Africa (e.g., Cassé et al. 2015, Sylla et al. 2015, Gosset et al. 2013). Despite the spread, the P-datasets are roughly consistent on the south-to-north decrease in the number of wet days. The dataset ensemble mean suggests a decrease rate of about 8 days per degree of latitude over the area from 5.5°N to 10.5°N and about 12.5 days per degree from 10.5°N to 18°N.

Over Burkina Faso, EPEs defined with the wet-day 96th percentile are similar to those defined with the all-day 99th percentile as used here above. For the highest quantiles, the spread in the wet-day rainfall distribution over pixel 3E (Fig. 14b) is similar to that found based on all days (Fig. 2a): the datasets, which overestimate or underestimate the rainfall quantiles are the same for both EPE definitions. The biases in the wet-day 96th percentile are approximately similar to those in the all-day 99th percentile (Fig. 14c). Nevertheless, rainfall products that overestimate the wet-day 96th (and all-day 99th) percentile are also those that under-represent the occurrence of wet days, and vice-versa.

The spatial distributions of both types of percentiles and their spread among P-datasets are also broadly similar at the scale of West Africa (Figs. 3 and 15). The meridional gradients are rather consistent, while the spread remains high for the zonal variations. Nevertheless, the sensitivity can be large at country or local scales, particularly south of the Sahel, where the north-to-south increase in the frequency of wet-day is strong (Fig. 14a). For instance the maximum of the all-day 99th percentile over the Sahel observed in CMORPH-CRT, GSMaP-gauge-RNL and GPCP-CDR is accentuated when considering the wet-day 96th percentile (Figs. 3 and 15). This maximum now appears in the wet-day 96th percentile of TMPA-3B42 and IMERG-FC, while it is fully absent in their all-day 99th percentile field.

Similar conclusions as in Section 4.b, 4.c and 4.d are found when using the 96th wet-day percentile: EPEs and monsoon rainfall are strongly coupled both at the seasonal (Fig. S29) and interannual timescale (not shown); the performance and rank of the P-datasets are similar for both approaches (Fig. S28). But, several subtle details emerge because of the significant spread in the wet-day frequency of occurrence. Regional or local studies requiring a wet-day percentile EPE definition thus deserve a specific caution in their interpretation, and will need further investigation to identify the most relevant datasets, if any.

b. Near-real-time P-datasets

Early assessment of the risk (e.g., flooding) associated with the occurrence of EPEs is crucial for appropriate early warning systems. Therefore, we focused in this section on the near-real-time (basically uncalibrated) P-datasets TMPA-3B42RT, CMORPH-Raw, IMERG-EU and IMERG-LU, GSMaP-no-gauge-NRT, GSMaP-gauge-NRT and CHIRP. The tendency of their research counterpart to overestimate EPE intensity is generally more pronounced (Fig. 16, see also Gosset et al. 2013; Jobard et al. 2011) except for CHIRP, which underestimate it in most of Burkinabe pixels. They also exhibit significant differences with their research version on the EPE spatial distribution (Figs. 17 and 3), emphasizing the role of the rain-gauge-based calibration. Nevertheless, the MW-based near real-time datasets suggest that EPEs are the most intense over the Sahel. This feature is significantly enhanced compared to that mentioned earlier for GPCP-CDR, GSMaP-gauge-RNL and CMORPH-CRT (Figs. 3 and 17). This questions the existence of this band of EPE maxima over the Sahel, and to what extent the bias correction of the research product versions, based on a weakly-dense rain-gauge network, may reduce or remove this specific pattern.

To conclude this section, GSMaP-gauge-NRT and CHIRP appear as the most relevant products for near-real-time application over Burkina Faso, and probably over most of the Sahel.

6. Conclusions:

The present study documents several features of EPEs over the Sahel using 24 gridded P-datasets with a focus on Burkina Faso where a high-density rain-gauge network is available as a reference dataset

EPEs are defined as daily rainfall events at the scale of a 1°x1° pixel, which exceed the 99th all-day percentile computed over 2001-2013 the longest common period to all the datasets considered. This definition implies a mean EPE occurrence of 3.65 events per year and per 1°x1° pixel. Over Burkina Faso, and based on our reference dataset, the 99th percentile values range between 21 mm day^{-1} and 33 mm day^{-1}, with a slight south-to-north decrease. EPEs contribute to approximately 16% of the total annual rainfall. Their seasonal and interannual variability is strongly coupled to the West African monsoon, and as such, they mostly occur during the monsoon core season (June to September) and during anomalously wet years. The interannual variability of the EPE contribution to total annual rainfall is mainly driven by the interannual variability of their frequency of occurrence, rather than by that of their intensity. Nevertheless, EPEs only account for a small proportion of the total rainfall interannual variability.

The consistency between the precipitation products on EPE properties is explored over Burkina Faso as well as the Western, Central and Eastern Sahel. Except for the EPE intensity for which the product spread is large, the previous description of EPEs is consistent across most datasets over Burkina Faso and over the wider Sahel. A noticeable regional difference is the larger spread found over the Western Sahel. To our knowledge this provides the first regional documentation of EPE intensity, annual cycle as well as their seasonal and interannual variability.

Overall very few datasets succeed to reproduce properly all these EPE features. GPCC-FDDv1 and GSMaP-gauge-RNL exhibit the highest agreement with the reference dataset and appears appropriate for studying EPEs over Burkina Faso. A few datasets also exhibit a reasonable skill on some of the EPE properties (e.g. IMERG-FC, CMORPH-CRT, REGEN and to a lesser extent CHIRPS, TMPA-3B42, GPCP-CDR). More specific conclusions are discussed in the following.

The spread of the EPE intensity is strong among the P-dataset. REGEN, GPCC-FDDv1, GSMaP-gauge-RNL, IMERG-FC, CMORPH-CRT appears the most realistic over Burkina Faso, within the reference uncertainty range. In general the MW+IR-based products overestimate the EPEs intensity, while products based on IR only underestimate it. The overestimation of the EPE intensity is more pronounced in MW+IR-based near-real-time products. Only GSMaP-gauge-NRT and CHIRP perform realistically over Burkina Faso and as this respect should be appropriate for near-real-time applications.

The spatial distribution of the EPE intensity over the Sahel significantly varies among the P-datasets, especially along the Sahara margins, the Guinean Coast and Highlands, the

Eastern Sahel and Central Africa. Despite these discrepancies, most of the datasets agree on a broad south-to-north decrease in EPE intensity.

The strong coupling between EPEs and the annual cycle of total rainfall is quantitatively captured by most of the datasets over Burkina Faso, SM2RAIN-CI, TAMSAT, PERSIANN-CDR and CHIRPS showing the largest biases. The interannual variability is a more critical feature to capture. Only GPCC-FDDv1, GSMaP-gauge-RNL and CMORPH-CRT adequately reproduce the observed EPE interannual variability, while being still skillful for their intensity. It should be noted that SM2RAIN-CI and TAMSAT should not be used for the study of EPEs.

The sensitivity of the results to the use of a wet-day percentile approach to define EPEs was also explored. The results summarized here above are qualitatively robust, but additional uncertainties are induced by differences in the number of wet days between P-datasets and between the various rainfall regimes of West Africa. This calls for caution when using such an approach (see also Schär et al. 2016), but also for further investigation depending on the targeted application.

This work provides a systematic documentation of EPEs over Burkina Faso, and to some extent over the Sahel. It now calls for investigation of the mechanisms associated in their occurrence and variability, in particular in terms of interaction with their large-scale environment. This may also guide future evaluation of EPEs in state-of-the-art general circulation models.

In Memoriam

During the final stages of this work, Dr. Françoise Guichard passed away suddenly and unexpectedly. Françoise significantly inspired this study in particular pushing hard for exploring the FROGS database. She was a big fan of ground observations, always questioning models and indirect observations. She contributed a lot to the interpretation and synthesis of the present results. Without her, this study, and the PhD which underlies it, would not have been possible. We are sure the final form of this paper would have had his full approval and that she would have been proud of it. It has been a pleasure and honor to work with Françoise. We will miss her deep knowledge of atmospheric science, her person, her kindness and her ability to make ground observations illuminates climate processes.

Acknowledgments.

S. Sanogo, P. Peyrillé and R. Roehrig acknowledge support from Météo-France in conducting this work. We thank A. H. Fink, G. Panthou, Philippe Chambon for fruitful discussions along this work and F. Favot for her help in collecting the data. We also thank the Agence Nationale de la Météorologie of Burkina Faso for providing the rain-gauge data, and R. Roca and his collaborators for developing the FROGS database. We strongly acknowledge the tremendous efforts of all the teams that develop the 24 gridded rainfall datasets used in this work. We would also like to thank Dr. S.-K. Min for editing this work, and Dr. B. S. Pickering and two anonymous reviewers for their constructive comments.

Data Availability Statement.

The gridded precipitation data used in this study are openly available at DOI: https://doi.org/10.14768/06337394-73A9-407C-9997-0E380DAC5598 except for MSWEP and RFE which are available at www.gloh2o.org and ftp://ftp.cpc.ncep.noaa.gov/fews/fewsdata/africa/rfe2/ respectively. The reference rain-gauge dataset used in this study has been made available by the Agence Nationale de la Météorologie (ANAM) of Burkina Faso within the frame of the World Meteorological

Organisation-CREWS (Climate Risk & Early Warning System) project over Burkina Faso (2018-2020). The rain-gauge data are available upon request to ANAM.

REFERENCES

AghaKouchak, A., A. Behrangi, S. Sorooshian, K. Hsu, et E. Amitai. 2011. Evaluation of Satellite-Retrieved Extreme Precipitation Rates across the Central United States. *Journal of Geophysical Research: Atmospheres* 116(D2). doi: https://doi.org/10.1029/2010JD014741.

Alexander, L. V., H. J. Fowler, M. Bador, A. Behrangi, M. G. Donat, R. Dunn, C. Funk, J. Goldie, E. Lewis, M. Rogé, S. I. Seneviratne, et V. Venugopal. 2019. On the Use of Indices to Study Extreme Precipitation on Sub-Daily and Daily Timescales. *Environmental Research Letters* 14(12):125008. doi: 10.1088/1748-9326/ab51b6.

Arkin, P. A., et B. N. Meisner. 1987. The Relationship between Large-Scale Convective Rainfall and Cold Cloud over the Western Hemisphere during 1982-84. *Monthly Weather Review* 115(1):51-74. doi: 10.1175/1520-0493(1987)115<0051:TRBLSC>2.0.CO;2.

Ashouri, H., K.-L. Hsu, S. Sorooshian, D. K. Braithwaite, K. R. Knapp, L. D. Cecil, B. R. Nelson, et O. P. Prat. 2015. PERSIANN-CDR: Daily Precipitation Climate Data Record from Multisatellite Observations for Hydrological and Climate Studies. *Bulletin of the American Meteorological Society* 96(1):69-83. doi: 10.1175/BAMS-D-13-00068.1.

Baldassarre, G. D., A. Montanari, H. Lins, D. Koutsoyiannis, L. Brandimarte, et G. Blöschl. 2010. Flood Fatalities in Africa: From Diagnosis to Mitigation. *Geophysical Research Letters* 37(22). doi: https://doi.org/10.1029/2010GL045467.

Beck, H. E., A. I. J. M. van Dijk, V. Levizzani, J. Schellekens, D. G. Miralles, B. Martens, and Ad Roo. 2017. MSWEP: 3-Hourly 0.25° Global Gridded Precipitation (1979-

2015) by Merging Gauge, Satellite, and Reanalysis Data. *Hydrology and Earth System Sciences* 21(1):589-615. doi: https://doi.org/10.5194/hess-21-589-2017.

Beck, H. E., A. I. J. M. van Dijk, A. d. Roo, E. Dutra, G. Fink, R. Orth, and J. Schellekens. 2017. Global Evaluation of Runoff from 10 State-of-the-Art Hydrological Models. *Hydrology and Earth System Sciences* 21(6):2881-2903. doi: 10.5194/hess-21-2881-2017.

Becker, A., P. Finger, A. Meyer-Christoffer, B. Rudolf, K. Schamm, U. Schneider, et M. Ziese. 2013. A Description of the Global Land-Surface Precipitation Data Products of the Global Precipitation Climatology Centre with Sample Applications Including Centennial (Trend) Analysis from 1901–Present. *Earth System Science Data* 5(1):71-99. doi: https://doi.org/10.5194/essd-5-71-2013.

Berthou, S., E. J. Kendon, D. P. Rowell, M. J. Roberts, S. Tucker, et R. A. Stratton. 2019. Larger Future Intensification of Rainfall in the West African Sahel in a Convection-Permitting Model. *Geophysical Research Letters* 46(22):13299-307. doi: https://doi.org/10.1029/2019GL083544.

Beucher, F., J.-P. Lafore, et N. Chapelon. 2020. Simulation and Analysis of the Moist Vortex Associated with the Extreme Rain Event of Ouagadougou in 2009. *Quarterly Journal of the Royal Meteorological Society* 146(726):86-104. doi: https://doi.org/10.1002/qj.3645.

Bower R. G., M. Goldstein, and I. Vernon. 2010. Galaxy formation: a bayesian uncertainty analysis. Bayesian Analysis, 5(4):619–669, (2010). doi: 10.1214/10-BA524. URL https://doi.org/10.1214/10-BA524.

Cassé, C., M. Gosset, C. Peugeot, V. Pedinotti, A. Boone, B. A. Tanimoun, et B. Decharme. 2015. Potential of Satellite Rainfall Products to Predict Niger River Flood Events in Niamey. *Atmospheric Research* 163:162-76. doi: 10.1016/j.atmosres.2015.01.010.

Chen, M., W. Shi, P. Xie, V. B. S. Silva, V. E. Kousky, R. W. Higgins, et J. E. Janowiak. 2008. Assessing Objective Techniques for Gauge-Based Analyses of Global Daily Precipitation. *Journal of Geophysical Research: Atmospheres* 113(D4). doi: https://doi.org/10.1029/2007JD009132.

Ciabatta, L., C. Massari, L. Brocca, A. Gruber, C. Reimer, S. Hahn, C. Paulik, W. Dorigo, R. Kidd, et W. Wagner. 2018. SM2RAIN-CCI: A New Global Long-Term Rainfall Data Set Derived from ESA CCI Soil Moisture. *Earth System Science Data* 10(1):267-80. doi: https://doi.org/10.5194/essd-10-267-2018.

Contractor, S., M. G. Donat, L. V. Alexander, M. Ziese, A. Meyer-Christoffer, U. Schneider, E. Rustemeier, A. Becker, I. Durre, et R. S. Vose. 2020. Rainfall Estimates on a Gridded Network (REGEN) – a Global Land-Based Gridded Dataset of Daily Precipitation from 1950 to 2016. *Hydrology and Earth System Sciences* 24(2):919-43. doi: 10.5194/hess-24-919-2020.

Crétat, J., E. Vizy, et K. H. Cook. 2013. How well are daily intense rainfall events captured by current climate models over Africa? *Climate Dynamics* 42:2691-2711. doi: 10.1007/s00382-013-1796-7.

Crétat, J., E. K. Vizy, et K. H. Cook. 2015. The Relationship between African Easterly Waves and Daily Rainfall over West Africa: Observations and Regional Climate Simulations. *Climate Dynamics* 44(1):385-404. doi: 10.1007/s00382-014-2120-x.

Descroix, L., F. Guichard, M. Grippa, L. Lambert, G. Panthou, G. Mahé, L. Gal, C. Dardel, G. Quantin, L. Kergoat, Y. Bouaïta, P. Hiernaux, T. Vischel, T. Pellarin, B. Faty, C. Wilcox, M. Malam Abdou, I. Mamadou, Jean-Pierre Vandervaere, A. Diongue-Niang, O. Ndiaye, Y. Sané, H. Dacosta, M. Gosset, C. Cassé, B. Sultan, A. Barry, O. Amogu, B. N. Nnomo, A. Barry, et Jean-Emmanuel Paturel. 2018. Evolution of Surface Hydrology in the Sahelo-Sudanian Strip: An Updated Review. *Water* 10(6):748. doi:

10.3390/w10060748.

Diaconescu, E. P., P. Gachon, J. Scinocca, et R. Laprise. 2015. Evaluation of Daily Precipitation Statistics and Monsoon Onset/Retreat over Western Sahel in Multiple Data Sets. *Climate Dynamics* 45(5):1325-54. doi: 10.1007/s00382-014-2383-2.

Diakhaté, M., B. Rodríguez-Fonseca, I. Gómara, E. Mohino, A. L. Dieng, et A. T. Gaye. 2019. Oceanic Forcing on Interannual Variability of Sahel Heavy and Moderate Daily Rainfall. *Journal of Hydrometeorology* 20(3):397-410. doi: 10.1175/JHM-D-18-0035.1.

Donat, Markus G., O.Angélil, et A. M. Ukkola. 2019. Intensification of Precipitation Extremes in the World's Humid and Water-Limited Regions. *Environmental Research Letters* 14(6):065003. doi: 10.1088/1748-9326/ab1c8e.

Efron, B., et R. J. Tibshirani. 1994. *An Introduction to the Bootstrap*. CRC Press.

Engel, T., A. H. Fink, P. Knippertz, G. Pante, et J. Bliefernicht. 2017. Extreme Precipitation in the West African Cities of Dakar and Ouagadougou: Atmospheric Dynamics and Implications for Flood Risk Assessments. *Journal of Hydrometeorology* 18(11):2937-57. doi: 10.1175/JHM-D-16-0218.1.

Fink, A. H., T. Engel, V. Ermert, R. van der Linden, M. Schneidewind, R. Redl, E. Afiesimama, W. M. Thiaw, C. Yorke, M. Evans, et S. Janicot. 2017. Mean Climate and Seasonal Cycle. P. 1-39 in *Meteorology of Tropical West Africa*. John Wiley & Sons, Ltd.

Funk, C., P. Peterson, M. Landsfeld, D. Pedreros, J. Verdin, S. Shukla, G. Husak, J. Rowland, L. Harrison, A. Hoell, et J. Michaelsen. 2015. The Climate Hazards Infrared Precipitation with Stations—a New Environmental Record for Monitoring Extremes. *Scientific Data* 2(1):150066. doi: 10.1038/sdata.2015.66.

Giorgi, F., E. S. Im, E. Coppola, N. S. Diffenbaugh, X. J. Gao, L. Mariotti, et Y. Shi. 2011.

Higher Hydroclimatic Intensity with Global Warming. *Journal of Climate* 24(20):5309-24. doi: 10.1175/2011JCLI3979.1.

Gosset, M., M. Alcoba, R. Roca, S. Cloché, et G. Urbani. 2018. Evaluation of TAPEER Daily Estimates and Other GPM-Era Products against Dense Gauge Networks in West Africa, Analysing Ground Reference Uncertainty. *Quarterly Journal of the Royal Meteorological Society* 144(S1):255-69. doi: https://doi.org/10.1002/qj.3335.

Gosset, M., J. Viarre, G. Quantin, et M. Alcoba. 2013. Evaluation of Several Rainfall Products Used for Hydrological Applications over West Africa Using Two High-Resolution Gauge Networks. *Quarterly Journal of the Royal Meteorological Society* 139(673):923-40. doi: https://doi.org/10.1002/qj.2130.

GSMaP Technical Documentation, 2014: Global Satellite Mapping of Precipitation (GSMaP) for GPM, Algorithm Theoretical Basis Document (ATBD) Algorithm Ver.6.

Herold, N., A. Behrangi, et L. V. Alexander. 2017. Large Uncertainties in Observed Daily Precipitation Extremes over Land. *Journal of Geophysical Research: Atmospheres* 122(2):668-81. doi: https://doi.org/10.1002/2016JD025842.

Huffman, G. J., R. F. Adler, P. Arkin, A. Chang, R. Ferraro, A. Gruber, J. Janowiak, A. McNab, B. Rudolf, et U. Schneider. 1997. The Global Precipitation Climatology Project (GPCP) Combined Precipitation Dataset. *Bulletin of the American Meteorological Society* 78(1):5-20. doi: 10.1175/1520-0477(1997)078<0005:TGPCPG>2.0.CO;2.

Huffman, G. J., R. F. Adler, M. M. Morrissey, D. T. Bolvin, S. Curtis, R. Joyce, B. McGavock, et J. Susskind. 2001. Global Precipitation at One-Degree Daily Resolution from Multisatellite Observations. *Journal of Hydrometeorology* 2(1):36-50. doi: 10.1175/1525-7541(2001)002<0036:GPAODD>2.0.CO;2.

Huffman, G. J., D. T. Bolvin, D. Braithwaite, K.-L. Hsu, R. J. Joyce, C. Kidd, E. J. Nelkin, S.

Sorooshian, E. F. Stocker, J. Tan, D. B. Wolff, et P. Xie. 2020. Integrated Multi-Satellite Retrievals for the Global Precipitation Measurement (GPM) Mission (IMERG). P. 343-53 in *Satellite Precipitation Measurement: Volume 1*, *Advances in Global Change Research*.

Huffman, G. J., D. T. Bolvin, E. J. Nelkin, D. B. Wolff, R. F. Adler, G. Gu, Y. Hong, K. P. Bowman, et E. F. Stocker. 2007. The TRMM Multisatellite Precipitation Analysis (TMPA): Quasi-Global, Multiyear, Combined-Sensor Precipitation Estimates at Fine Scales. *Journal of Hydrometeorology* 8(1):38-55. doi: 10.1175/JHM560.1.

Jobard, I., F. Chopin, J. C. Berges, et R. Roca. 2011. An intercomparison of 10-day satellite precipitation products during West African monsoon . *International Journal of Remote Sensing* 32(9):2353-76. doi: 10.1080/01431161003698286.

Jones, P. W. 1999. First- and Second-Order Conservative Remapping Schemes for Grids in Spherical Coordinates. *Monthly Weather Review* 127(9):2204-10. doi: 10.1175/1520-0493(1999)127<2204:FASOCR>2.0.CO;2.

Joyce, R., J. Janowiak, P. Arkin, et P. Xie. 2004. CMORPH: A Method That Produces Global Precipitation Estimates From Passive Microwave and Infrared Data at High Spatial and Temporal Resolution. *Journal of Hydrometeorology - J HYDROMETEOROL* 5. doi: 10.1175/1525-7541(2004)005<0487:CAMTPG>2.0.CO;2

Kubota, T., S. Shige, H. Hashizume, K. Aonashi, N. Takahashi, S. Seto, M. Hirose, Y. N. Takayabu, T. Ushio, K. Nakagawa, K. Iwanami, M. Kachi, et K. Okamoto. 2007. Global Precipitation Map Using Satellite-Borne Microwave Radiometers by the GSMaP Project: Production and Validation. *IEEE Transactions on Geoscience and Remote Sensing* 45(7):2259-75. doi: 10.1109/TGRS.2007.895337.

Lafore, J.-P., F. Beucher, P. Peyrillé, A. Diongue-Niang, N. Chapelon, D. Bouniol, G. Caniaux, F. Favot, F. Ferry, F. Guichard, E. Poan, R. Roehrig, et T. Vischel. 2017. A

Multi-Scale Analysis of the Extreme Rain Event of Ouagadougou in 2009. *Quarterly Journal of the Royal Meteorological Society* 143(709):3094-3109. doi: https://doi.org/10.1002/qj.3165.

Laurent, H., N. D'Amato, et T. Lebel. 1998. How Important Is the Contribution of the Mesoscale Convective Complexes to the Sahelian Rainfall? *Physics and Chemistry of the Earth* 23(5):629-33. doi: 10.1016/S0079-1946(98)00099-8.

Lebel, T., et A. Amani. 1999. Rainfall Estimation in the Sahel: What Is the Ground Truth? *Journal of Applied Meteorology and Climatology* 38(5):555-68. doi: 10.1175/1520-0450(1999)038<0555:REITSW>2.0.CO;2.

Maidment, R. I., D. Grimes, E. Black, E. Tarnavsky, M. Young, H. Greatrex, R. P. Allan, T. Stein, E. Nkonde, S. Senkunda, et E. M. U. Alcántara. 2017. A New, Long-Term Daily Satellite-Based Rainfall Dataset for Operational Monitoring in Africa. *Scientific Data* 4(1):170063. doi: 10.1038/sdata.2017.63.

Mahalanobis P.C., On the generalised distance in statistics Proceedings of the National Institute of Sciences of India, 2(1):49–55, 1936.

Masunaga, H., M. Schröder, F. A. Furuzawa, C. Kummerow, E. Rustemeier, et U. Schneider. 2019. Inter-Product Biases in Global Precipitation Extremes. *Environmental Research Letters* 14(12):125016. doi: 10.1088/1748-9326/ab5da9.

Mathon, V., H. Laurent, et T. Lebel. 2002. Mesoscale Convective System Rainfall in the Sahel. *Journal of Applied Meteorology and Climatology* 41(11):1081-92. doi: 10.1175/1520-0450(2002)041<1081:MCSRIT>2.0.CO;2.

Nicholson, S. E., B. Some, J. McCollum, E. Nelkin, D. Klotter, Y. Berte, B. M. Diallo, I. Gaye, G. Kpabeba, O. Ndiaye, J. N. Noukpozounkou, M. M. Tanu, A. Thiam, A. A. Toure, et A. K. Traore. 2003a. Validation of TRMM and Other Rainfall Estimates with a High-Density Gauge Dataset for West Africa. Part I: Validation of GPCC

Rainfall Product and Pre-TRMM Satellite and Blended Products. *Journal of Applied Meteorology and Climatology* 42(10):1337-54. doi: 10.1175/1520-0450(2003)042<1337:VOTAOR>2.0.CO;2.

Nicholson, S. E., B. Some, J. McCollum, E. Nelkin, D. Klotter, Y. Berte, B. M. Diallo, I. Gaye, G. Kpabeba, O. Ndiaye, J. N. Noukpozounkou, M. M. Tanu, A. Thiam, A. A. Toure, et A. K. Traore. 2003b. Validation of TRMM and Other Rainfall Estimates with a High-Density Gauge Dataset for West Africa. Part II: Validation of TRMM Rainfall Products. *Journal of Applied Meteorology and Climatology* 42(10):1355-68. doi: 10.1175/1520-0450(2003)042<1355:VOTAOR>2.0.CO;2.

Novella, N. S., et W. M. Thiaw. 2013. African Rainfall Climatology Version 2 for Famine Early Warning Systems. *Journal of Applied Meteorology and Climatology* 52(3):588-606. doi: 10.1175/JAMC-D-11-0238.1.

Odoulami, R., et A. Akinsanola. 2018. Recent assessment of West African summer monsoon daily rainfall trends. *Weather* 73:283-87. doi: 10.1002/wea.2965.

Panthou, G., T. Vischel, et T. Lebel. 2014. Recent Trends in the Regime of Extreme Rainfall in the Central Sahel. *International Journal of Climatology* 34(15):3998-4006. doi: https://doi.org/10.1002/joc.3984.

Reynolds, R. W. 1988. A Real-Time Global Sea Surface Temperature Analysis. *Journal of Climate* 1(1):75-87. doi: 10.1175/1520-0442(1988)001<0075:ARTGSS>2.0.CO;2.

Roca, R., L. V. Alexander, G.Potter, M. Bador, R. Jucá, S. Contractor, M. G. Bosilovich, et S. Cloché. 2019. FROGS: A Daily 1° × 1° Gridded Precipitation Database of Rain Gauge, Satellite and Reanalysis Products. *Earth System Science Data* 11(3):1017-35. doi: https://doi.org/10.5194/essd-11-1017-2019.

Roca, R., P. Chambon, I. Jobard, P.-E. Kirstetter, M. Gosset, et J. C. Bergès. 2010. Comparing Satellite and Surface Rainfall Products over West Africa at

Meteorologically Relevant Scales during the AMMA Campaign Using Error Estimates. *Journal of Applied Meteorology and Climatology* 49(4):715-31. doi: 10.1175/2009JAMC2318.1.

Salter J.M., D. B. Williamson, J. Scinocca, and V. Kharin. 2019. Uncertainty quantification for computer models with spatial out-put using calibration-optimal bases. Journal of the American Statisti-cal Association, 114(528):1800–1814, 2019. doi: 10.1080/01621459.2018.1514306.

Satgé, F., D. Defrance, B. Sultan, M.-P. Bonnet, F. Seyler, N. Rouché, F. Pierron, et J.-. Paturel. 2020. Evaluation of 23 Gridded Precipitation Datasets across West Africa. *Journal of Hydrology* 581:124412. doi: 10.1016/j.jhydrol.2019.124412.

Schär, C., N. Ban, E. M. Fischer, J. Rajczak, J. Schmidli, C. Frei, F. Giorgi, T. R. Karl, E. J. Kendon, A. M. G. K. Tank, P. A. O’Gorman, J. Sillmann, X. Zhang, et F. W. Zwiers. 2016. Percentile Indices for Assessing Changes in Heavy Precipitation Events. *Climatic Change* 137(1):201-16. doi: 10.1007/s10584-016-1669-2.

Sultan, B., et S. Janicot. 2000. Abrupt Shift of the ITCZ over West Africa and intra-seasonal variability. *Geophysical Research Letters* 2720:3353-56. doi: 10.1029/1999GL011285.

Sultan, B., et S. Janicot. 2003. The West African Monsoon Dynamics. Part II: The “Preonset” and “Onset” of the Summer Monsoon. *Journal of Climate* 16(21):3407-27. doi: 10.1175/1520-0442(2003)016<3407:TWAMDP>2.0.CO;2.

Sun, Q., C. Miao, Q. Duan, H. Ashouri, S. Sorooshian, et K.-L. Hsu. 2018. « A Review of Global Precipitation Data Sets: Data Sources, Estimation, and Intercomparisons ». *Reviews of Geophysics* 56(1):79-107. doi: https://doi.org/10.1002/2017RG000574.

Sylla, M. B., F. Giorgi, E. Coppola, et L. Mariotti. 2013. Uncertainties in Daily Rainfall over Africa: Assessment of Gridded Observation Products and Evaluation of a Regional

Climate Model Simulation. *International Journal of Climatology* 33(7):1805-17. doi: https://doi.org/10.1002/joc.3551.

Ta, S., K. Y. Kouadio, K. E. Ali, E. Toualy, A. Aman, et F. Yoroba. 2016. West Africa Extreme Rainfall Events and Large-Scale Ocean Surface and Atmospheric Conditions in the Tropical Atlantic. *Advances in Meteorology* 2016:e1940456. Doi: 10.1155/2016/1940456.

Tarhule, A. 2004. Damaging rainfall and flooding: the other Sahel hazards. Climatic Change (2005) 72: 355–377. doi: 10.1007/s10584-005-6792-4

Taupin, J., A. Amani, et T. Lebel. 1998. Variabilité spatiale des pluies au sahel: Une question d' échelles. Water Resources Variability in Africa during the XXth Century (Proceedings of the Abidjan' 98 Conference held at Abidjan, Côte d'lvoire, November 1998).

Taylor, C. M., D. Belušić, F. Guichard, D. J. Parker, T. Vischel, O. Bock, P. P. Harris, S. Janicot, C. Klein, et G. Panthou. 2017. Frequency of extreme Sahelian storms tripled since 1982 in satellite observations. *Nature* 544(7651):475-78. doi: 10.1038/nature22069.

Williamson D., A.T. Blaker, C. Hampton, and J. Salter. 2019. Identifying and removing structural biases in climate models with history matching. Climate Dynamics, 45(5):1299–1324, 2015. doi: 10.1007/s00382-014-2378-z.

Xie, P., R. Joyce, S. Wu, S.-H. Yoo, Y. Yarosh, F. Sun, et R. Lin. 2017. Reprocessed, Bias-Corrected CMORPH Global High-Resolution Precipitation Estimates from 1998. *Journal of Hydrometeorology* 18(6):1617-41. doi: 10.1175/JHM-D-16-0168.1.

Ziese, Markus, Armin Rauthe-Schöch, Andreas Becker, Peter Finger, Anja Meyer-Christoffer, et Udo Schneider. 2018. GPCC Full Data Daily Version 2018 at 1.0°: Daily Land-Surface Precipitation from Rain-Gauges built on GTS-based and Historic

Data: Gridded Daily Totals. 40 MB per annual gzip compressed NetCDF archive.

Zhang, X., L. Alexander, G. C. Hegerl, P. Jones, A. K. Tank, T. C. Peterson, B. Trewin, et F. W. Zwiers. 2011. Indices for Monitoring Changes in Extremes Based on Daily Temperature and Precipitation Data. *WIREs Climate Change* 2(6):851-70. doi: https://doi.org/10.1002/wcc.147.

TABLES

Products short name and version	Products full name	Input data	Bias correction with rain-gauge data	Temporal coverage		Native spatial resolution	Latency	References
				Entire period	Longest period used in this study			
ARC v2	**Africa rainfall climatology version 2**	***Satellite (IR), Gauge***	***Daily***	***1983-present***	***1995-2016***	***0.1°***	***2 days***	***Novella et Thiaw (2013)***
CHIRP v2.0	Climate Hazards Group InfraRed version 2	Satellite (IR), Reanalysis	--	1981-present	1995-2016	0.05°	2 days	Funk et al. (2015)
CHIRPS v2.0	**Climate Hazards Group InfaRed precipitation with Stations version 2**	***Satellite (IR), Reanalysis, Gauge***	***Monthly, pentadal***	***1981-present***	***1995-2016***	***0.05°***	***1 month***	***Funk et al. (2015)***
CMORPH CRT v1.0	**Climate prediction Center MORPhing biais corrected version v1.0**	***Satellite (MW, IR), Gauge***	***Daily***	***1998-present***	***1998-2016***	***0.25°***	***6 month***	***Xie et al. (2017)***
CMORPH Raw v1.0	Climate prediction Center MORPhing Raw version v1.0	Satellite (MW, IR)	--	1998-present	1998-2016	0.25°	18 hours	Joyce et al. (2014)
GPCP 1DD CDR v1.3	**Global Precipitation Climatology Product (GPCP) Climate Data Record (CDR) Version 1.3**	***Satellite (MW, IR), Gauge***	***Monthly***	***1996-present***	***1997-2016***	***1°***	***Irregular***	***Huffman et al. (2001)***
GSMaP-gauge-NRT v6.0	Global Satellite Maping of Precipitation gauge Near-Real-Time version 6.0	Satellite (MW, IR), Gauge	--	2000-present	2001-2013	0.1	4 hours	Kubota et al. (2007)
GSMaP-no-gauge -NRT v6.0	Global Satellite Maping of Precipitation no gauge Near-Real-Time version 6.0	Satellite (MW, IR)	--	2000-present	2001-2013	0.1	4 hours	Kubota et al. (2007)
GSMaP- gauge-RNL v6.0	**Global Satellite Maping of Precipitation gauge Reanalysis version 6.0**	***Satellite (MW, IR), Gauge***	***Daily***	***2000-2014***	***2001-2013***	***0.1***	***irregular***	***Kubota et al. (2007)***

IMERG EU v6.0	Integrated Multi-satellitE Retrievals for Global Precipitation Measurement (GPM) Early Ucalibrated version 6.0	Satellite (MW, IR)	--	2000-present	2001-2013	0.1°	4 hours	Huffman et al. (2020)
IMERG FC v6.0	**Integrated Multi-satellitE Retrievals for Global Precipitation Measurement (GPM) final calibrated version 6.0**	***Satellite (MW, IR), Gauge***	***Monthly***	***2000-present***	***2001-2013***	***0.1°***	***3.5 months***	***Huffman et al. (2020)***
IMERG LU v6.0	Integrated Multi-satellitE Retrievals for (GPM) late Ucalibrated version 6.0	Satellite (MW, IR)	--	2000-present	2001-2013	0.1°	14 hours	Huffman et al. (2020)
MSWEP v1.2	**Multi-Source Weighted-Ensemble Precipitation (MSWEP) version 1.2**	***Satellite (MW, IR), Reanalysis, Gauge***	***Monthly, daily***	***1979-2015***	***1995-2016***	***0.25°***	***Irregular***	***Beck et al. (2017)***
PERSIANN CDR v1 r1	**Precipitation Estimation from Remotely Sensed Information using Artificial Neural Networks for Climate Data**	***Satellite (IR), Gauge***	***--***	***1983-present***	***1995-2016***	***0.25°***	***6 months***	***Ashouri et al. (2015)***
RFE v2	**Rainfall Estimation version 2.0**	***Satellite (IR, MW), Gauges***	***Daily***	***2001-present***	***2001-2016***	***0.1°***	***2 days***	***Novella et Thiaw (2013)***
SM2RAIN-CCI	**Soil Moisture to Rain applied on ESA Climate change Initiative**	***Satellite (MW), Gauge***	***--***	***1998-2015***	***1998-2015***	***0.25***	***Irregular***	***Ciabatta et al. (2018)***
TAMSAT v3	**The Tropical Applications of Meteorology using SATellite data and ground-based observations version 3.0**	***Satellite (IR), Gauge***	***--***	***1983-present***	***1995-2016***	***0.0375***	***3 days***	***Maidment et al. (2017)***
TMPA 3B42 v7	**TRMM Multi-satellite Precipitation Analysis 3B42 version 7**	***Satellite (MW, IR) Gauge***	***Monthly***	***1998-2019***	***1998-2016***	***0.25***	***stopped***	***Huffman et al. (2020)***
TMPA 3B42RT v7	TRMM Multi-satellite Precipitation Analysis 3B42 Near-Reail-Time version 7	Satellite (MW, IR)	--	2000-present	2001-2013	0.25	stopped	Huffman et al. (2020)

Table 1: The satellite-based P-datasets. The research (calibrated) products are emphasized in bold and italic fonts.

Products short name and version	**Products full name**	**Temporal coverage**		**Native spatial resolution**	**Latency**	**References**
		Entire period	**Longest period used in this study**			
CPC	Climate Prediction Centre	1979-present	1995-2016	0.5°	1-2 days	Chen et al. (2008)
GPCC-FDD v1	Global Precipitation Climatology Centre Full Data Daily version 1	1988-2013	1995-2013	1°	irregular	Becker et al. (2013)
GPCC-FDD v2018	Global Precipitation Climatology Centre Full Data Daily version 2018	1982-2016	1995-2016	1°	irregular	Ziese et al. (2018)
REGEN_AllStns_V1 (REGEN)	Rainfall Estimate on a GriddEd Network All Stations version 1	1950-2016	1995-2016	1°	irregular	Contractor et al. (2020)
REGEN_LongTermStns_V1 (REGEN40YR)	Rainfall Estimate on a GriddEd Network Long Term Stations version 1	1950-2016	1995-2016	1°	irregular	Contractor et al. (2020)

Table 2: *The rain-gauge-based P-datasets*

FIGURES

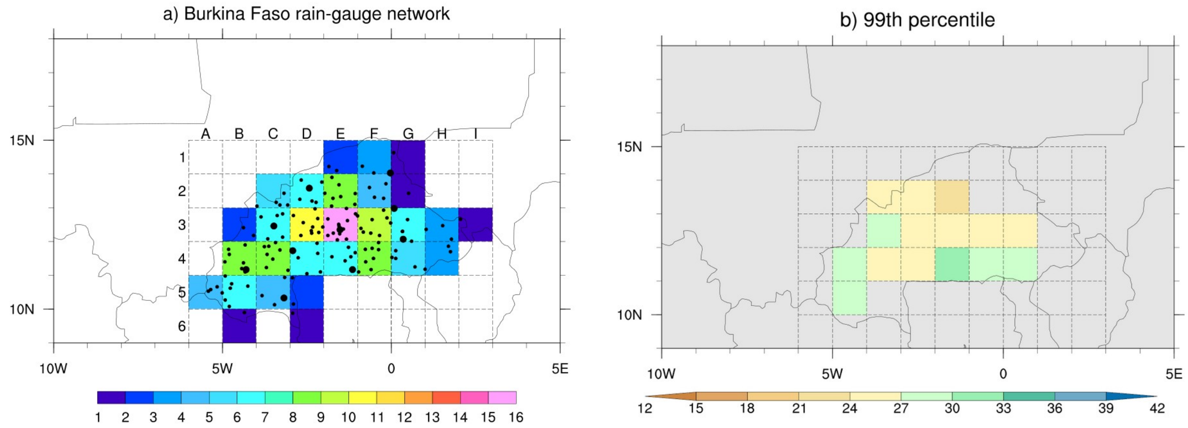

Figure 1: (a) Rain-gauge network over Burkina Faso used in the study (black dots) and number of stations per 1°x1° pixel (shading). Larger black dots highlight GTS rain-gauge stations. (b) All-day 99th percentile of daily rainfall (mm day^{-1}) for each 1°x1° pixel encompassing at least 5 rain-gauge stations (see text for details). The percentile is computed over the period 2001-2013.

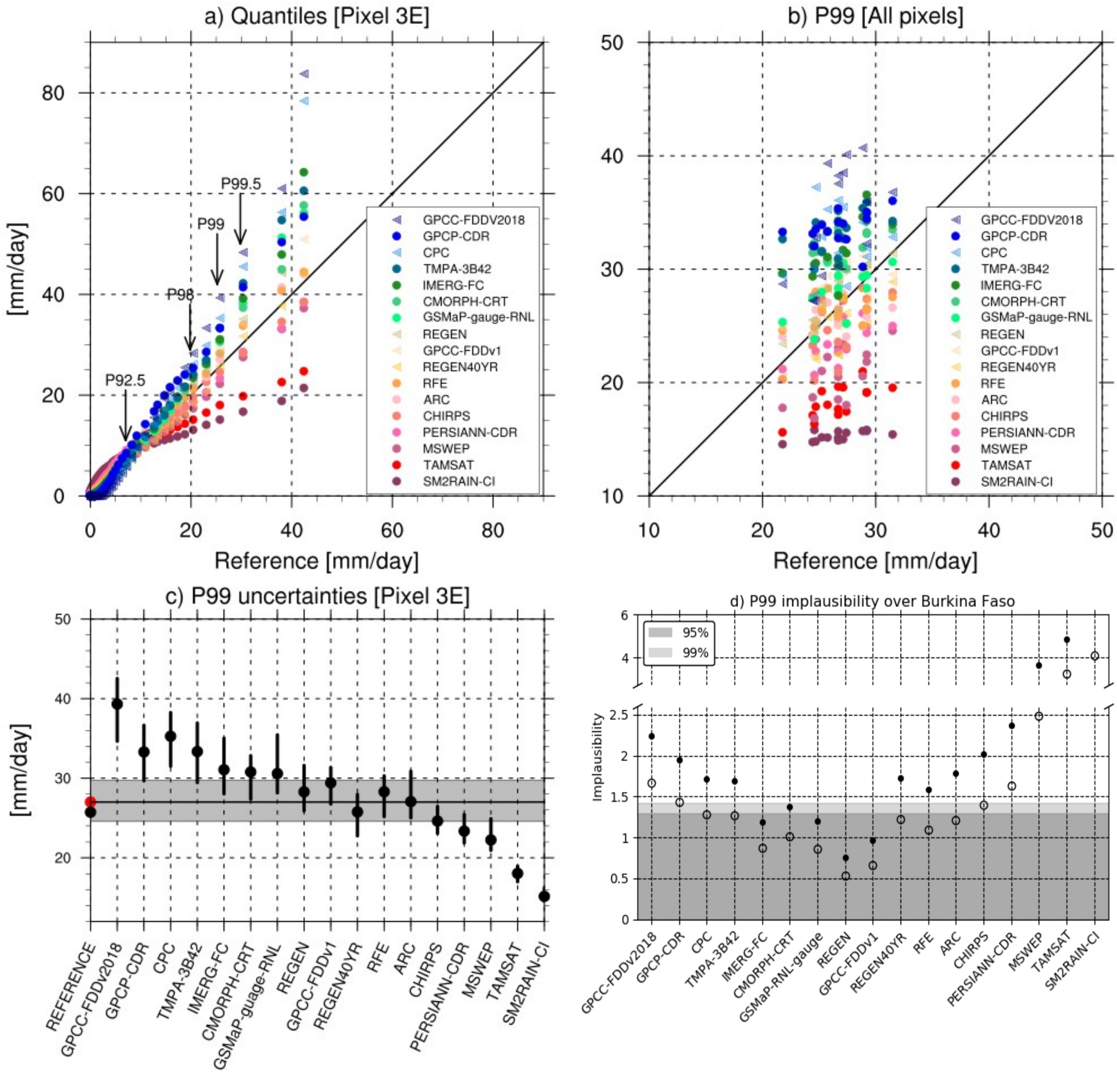

Figure 2: (a) Quantile-quantile plot of daily precipitation over the 1°x1° pixel 3E (Figure 1a). The x-axis corresponds to the reference dataset built from the rain-gauge network displayed on Figure 1a, while the y-axis corresponds to the precipitation gridded datasets evaluated in the present study. The last quantile shown on the scatter plot corresponds to the 99.9th quantile. (b) Scatter plot between the 99th percentile of the reference dataset (x-axis) and each of the evaluated P-dataset (y-axis), for the 15 1°x1° pixels covering Burkina Faso and

encompassing more than 5 rain-gauge stations. (c) The 99th percentile raw value of pixel 3E daily precipitation (black dots) and associated uncertainty range at the 95 % confidence level (vertical red segment) for each of the evaluated P-dataset (see text for details). For the reference dataset the black dot represents the 99th percentile raw value, the red dot and horizontal black line represent the bootstrap median 99th value and the grey shading its uncertainty range at the 95 % confidence level. (d) Implausibility for the 99th percentiles of the 15 1°x1° pixels of Figure 1b, evaluated for each P-dataset (see text for details). The dark and light grey shadings indicate respectively the 95% and 99% confidence levels that a given dataset is consistent with the reference dataset over the 15 pixels given the quantified sources of uncertainty. Filled and open dots correspond to a tolerance to error of 5% and 10% respectively.

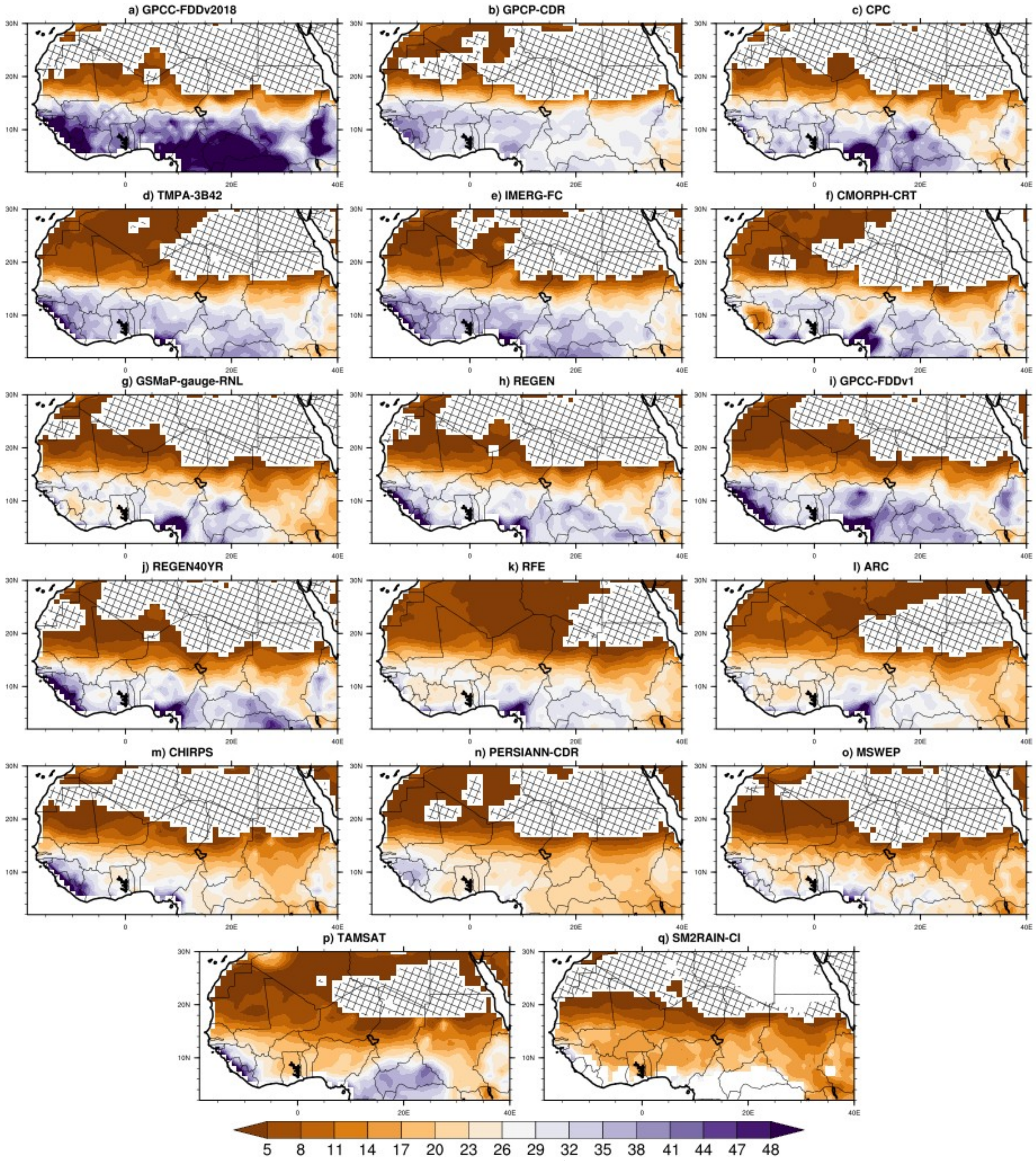

Figure 3: Spatial distribution of the all-day 99th percentile computed for each P-dataset. Hatching indicates pixels with less than 100 days with precipitation above 1 mm day^{-1} over the period 2001-2013. The white color for the SM2RAIN-CI dataset corresponds to pixels where no rainfall estimate is provided.

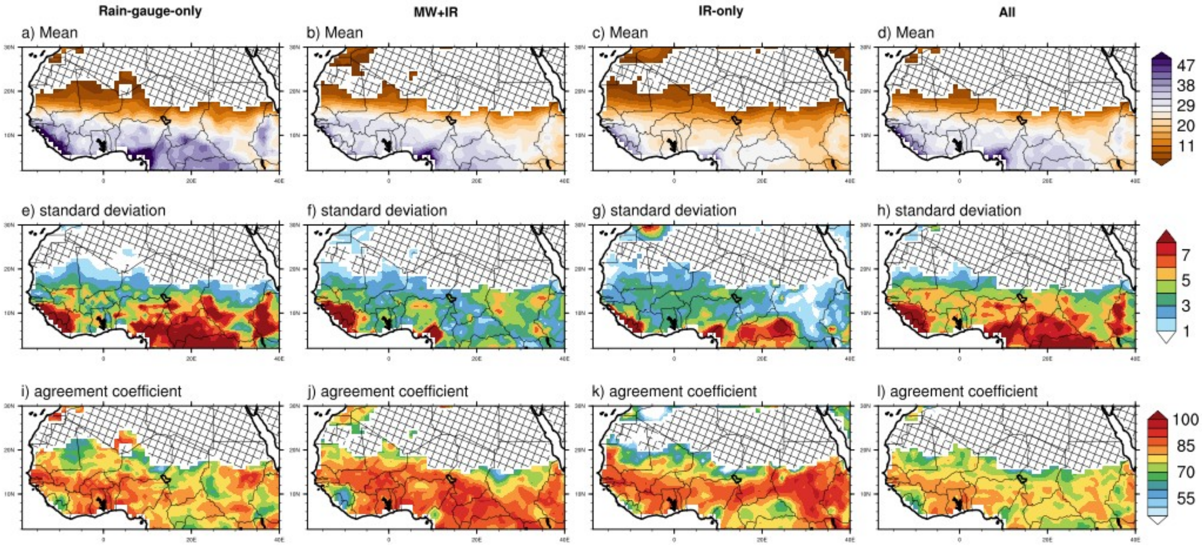

Figure 4: Mean (mm day^{-1}, a-d), standard deviation (mm day^{-1}, e-h) and coefficient of agreement (%, i-l, see text for detail) of the all-day 99th percentile of daily precipitation for different subsets of the evaluated datasets : rain-gauge-only (a, e, i), MW+IR (b, f, j), IR-only (c, g, k) and all (d, h, l) datasets. Note SM2RAIN-CI is not considered is any of these subsets, and MSWEP is only included in the all dataset diagnostics. Hatching indicates pixels with less than 100 days with precipitation above 1 mm day^{-1} over the period 2001-2013.

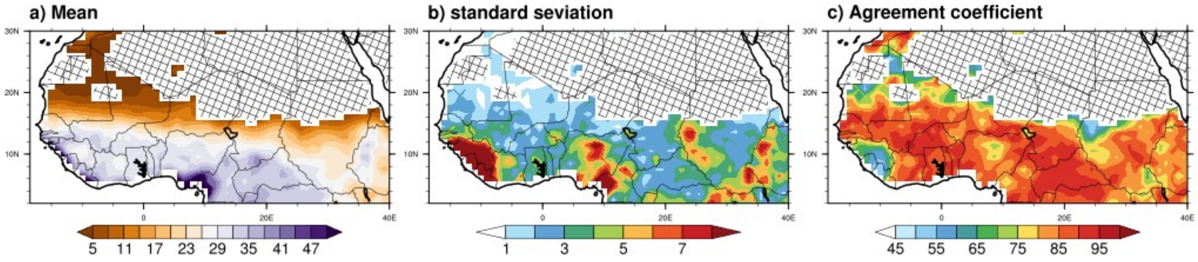

Figure 5: Same as Figure 4 but for the subset of P-datasets which are consistent with the reference dataset over Burkina Faso. The subset includes CMORPH-CRT, GPCC-FDDv1, GSMaP-gauge-RNL, IMERG-FC and REGEN.

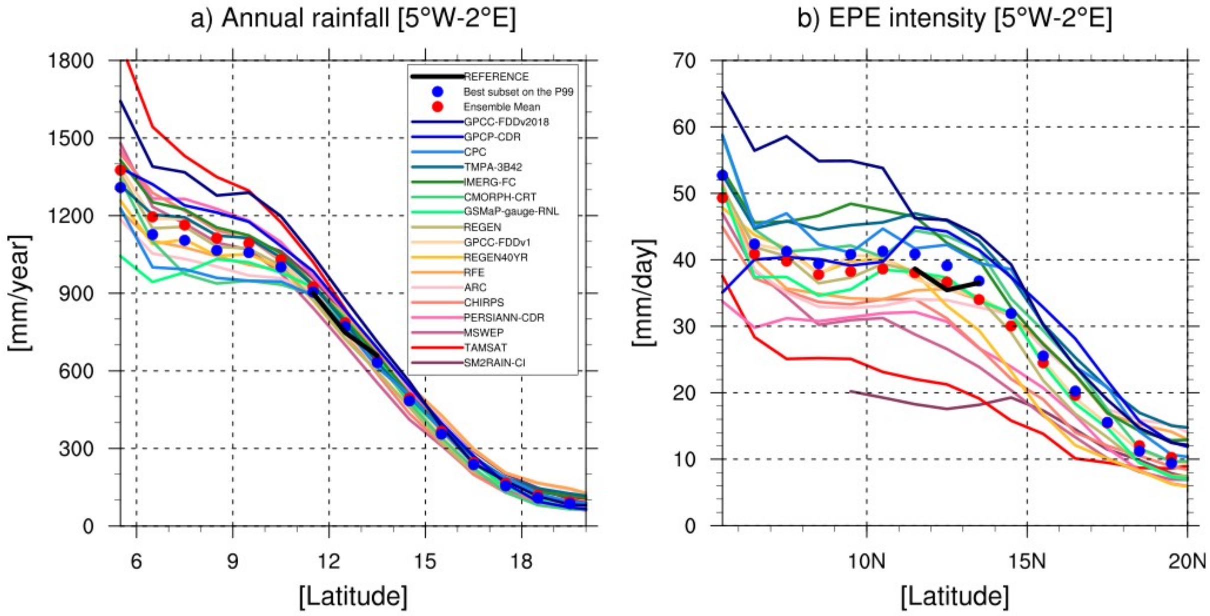

Figure 6: Meridional profile of (a) mean annual rainfall (mm year^{-1}) and (b) EPE-intensity (mm day^{-1}) for the evaluated P-datasets (colored lines), the reference dataset (thick black line), the ensemble mean over all the P-datasets except SM2RAIN-CI (red dots), and the ensemble mean over the P-datasets which are consistent with the reference dataset over Burkina Faso (blue dots). The two precipitation diagnostics are averaged over the 5°W-2°E longitude band.

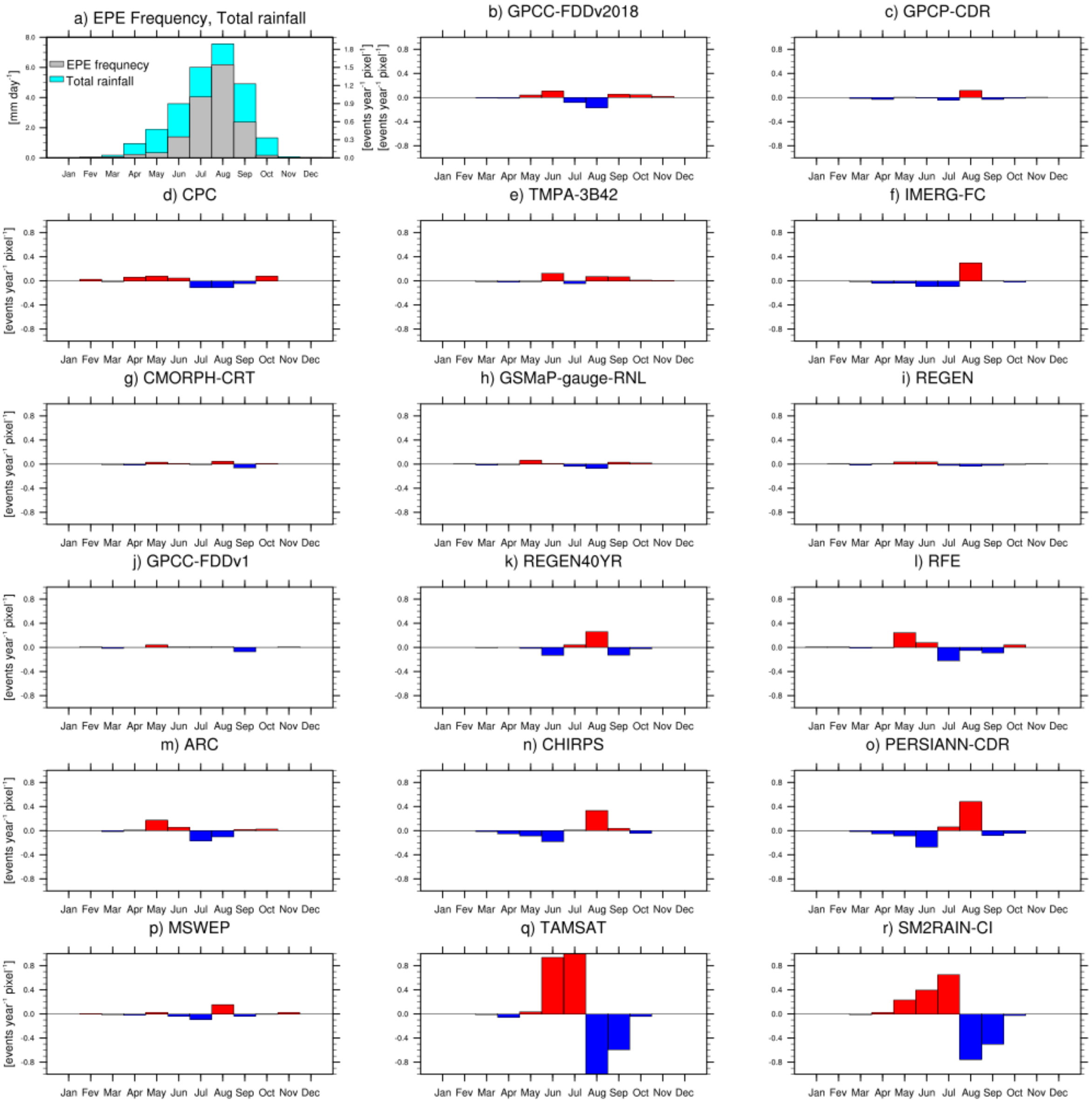

Figure 7: (a) Annual cycle of the EPE frequency of occurrence (events year^{-1} pixel^{-1}, grey bars) and total rainfall (mm day^{-1}, cyan bars) averaged over the 15 pixels covering Burkina Faso (Fig. 1b) and the period 2001-2013. (b-r) Annual cycle bias of the EPE frequency of occurrence for each of the evaluated P-dataset. The bias is computed against the reference datasets and averaged over the 15 pixels covering Burkina Faso and the period 2001-2013. The diagnostics are computed on a monthly basis.

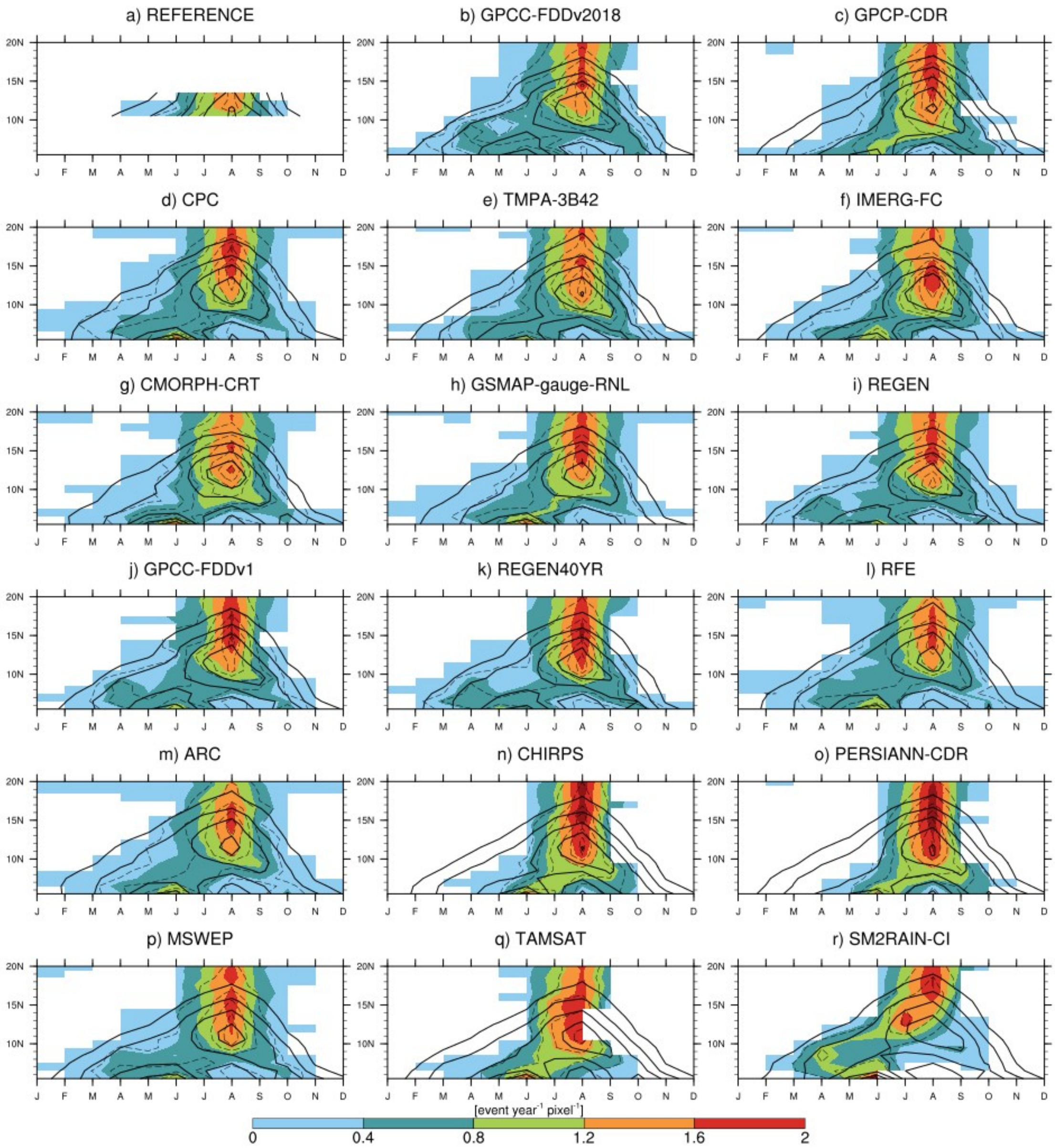

Figure 8: Time-latitude Hovmöller diagram of total rainfall (mm year^{-1}, solid contours, one contour every 50 mm year^{-1}, starting at 0 mm year^{-1}), EPE precipitation (mm year^{-1}, dashed contours, one contour every 10 mm year^{-1} starting at 0 mm year^{-1}) and EPE frequency of occurrence (events year^{-1} pixel^{-1}, shading). The diagnostics are averaged over the 5°W -2°E longitude band and the period 2001-2013, and computed on a monthly basis. The reference over Burkina Faso is shown on panel (a) and panels (b-r) correspond to the evaluated P-datasets. The white color indicates a zero frequency of occurrence.

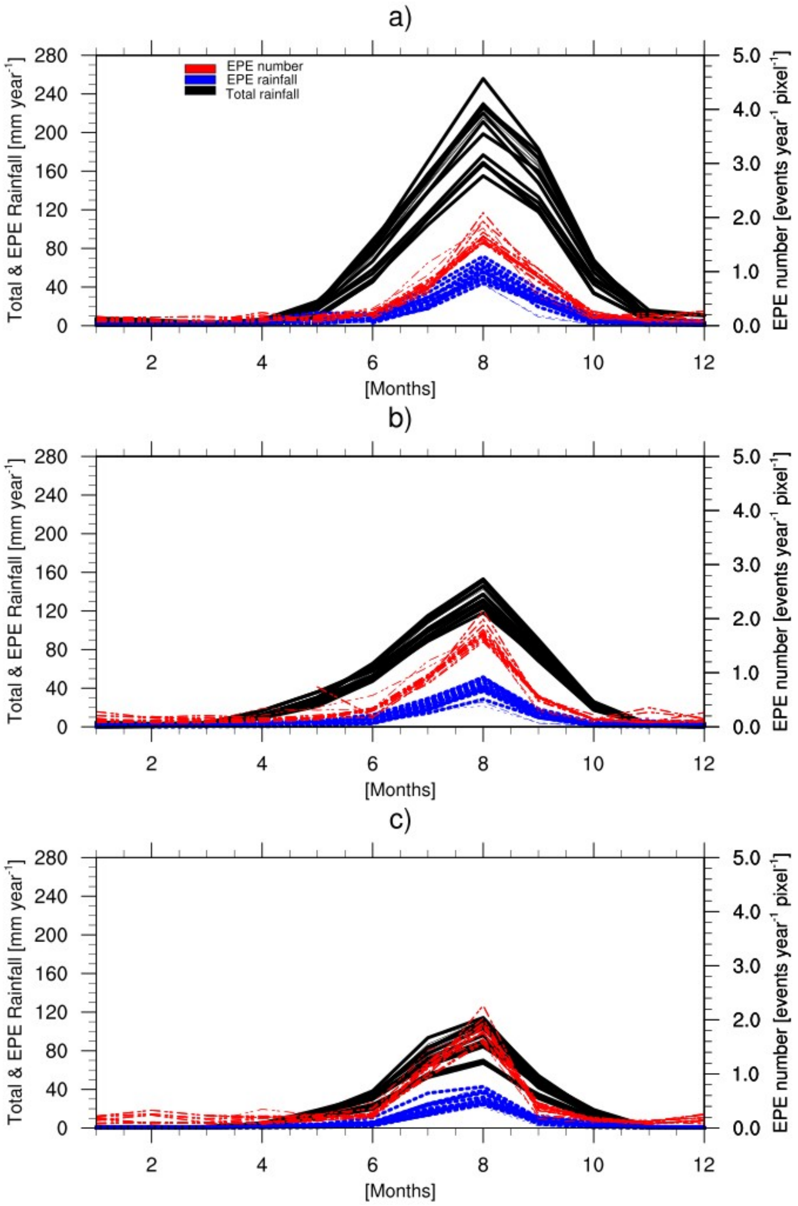

Figure 9: Mean annual cycle of total rainfall (solid, mm year^{-1}), EPE precipitation (blue, mm year^{-1}) and the EPE frequency of occurrence (red dashed, events year^{-1} pixel^{-1}) over the period 2001-2013 for (a) the Western Sahel [10°N-20°N, 17°W-10°W], (b) the Central Sahel [10°N-20°N, 10°W-15°E] and (c) the Eastern Sahel [10°N:-20°N, 15°E-35°E]. Each line corresponds to a given P-dataset.

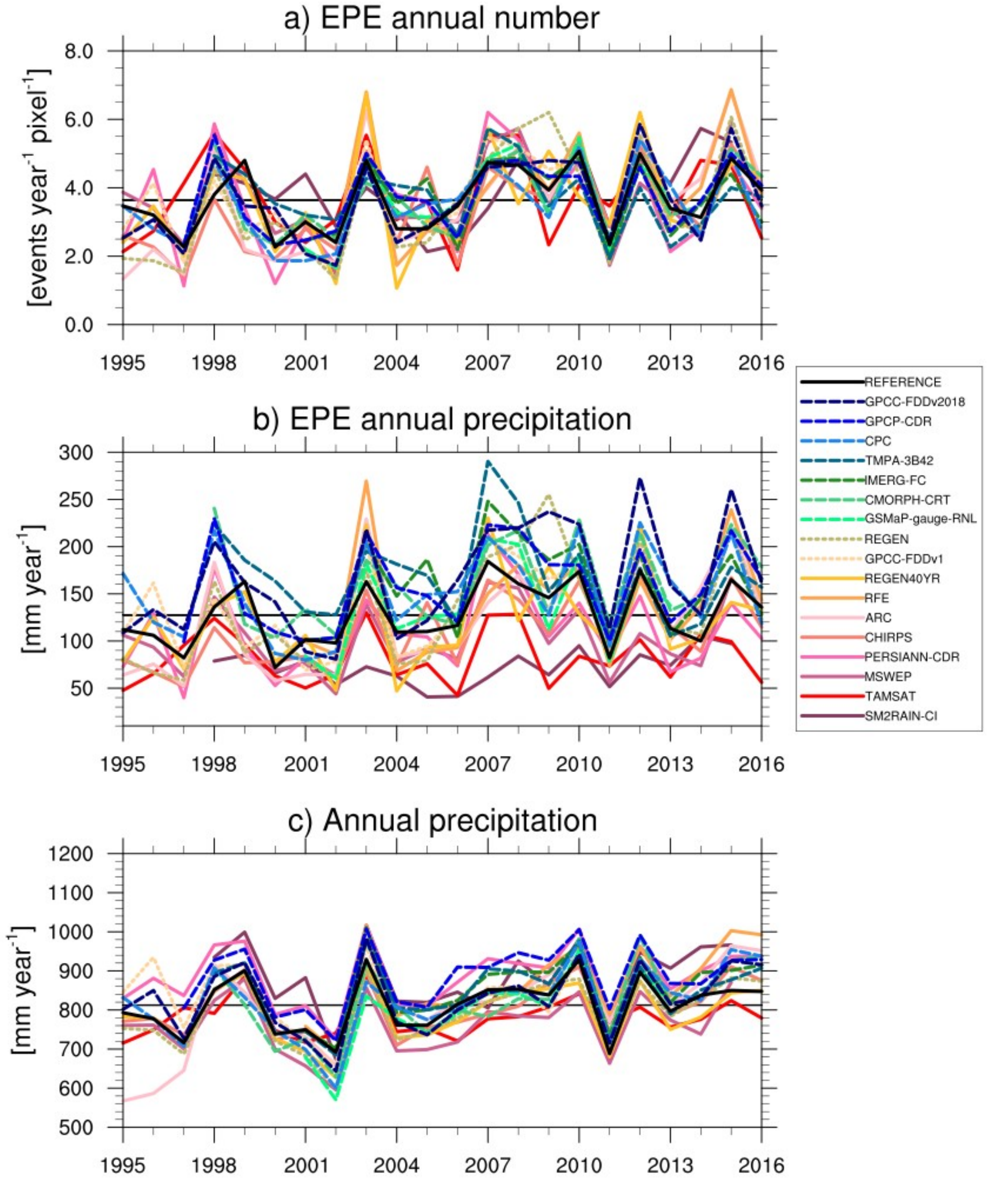

Figure 10: Time series of (a) the annual number of EPEs (events year^{-1}, pixel^{-1}), (b) the annual precipitation associated with EPEs (mm year^{-1}), and (c) the annual precipitation (mm year^{-1}). Over each panel, the horizontal black line indicates the long term mean of the diagnostic for the reference dataset. All diagnostics are averaged over the 15 pixels covering Burkina Faso (Fig. 1b).

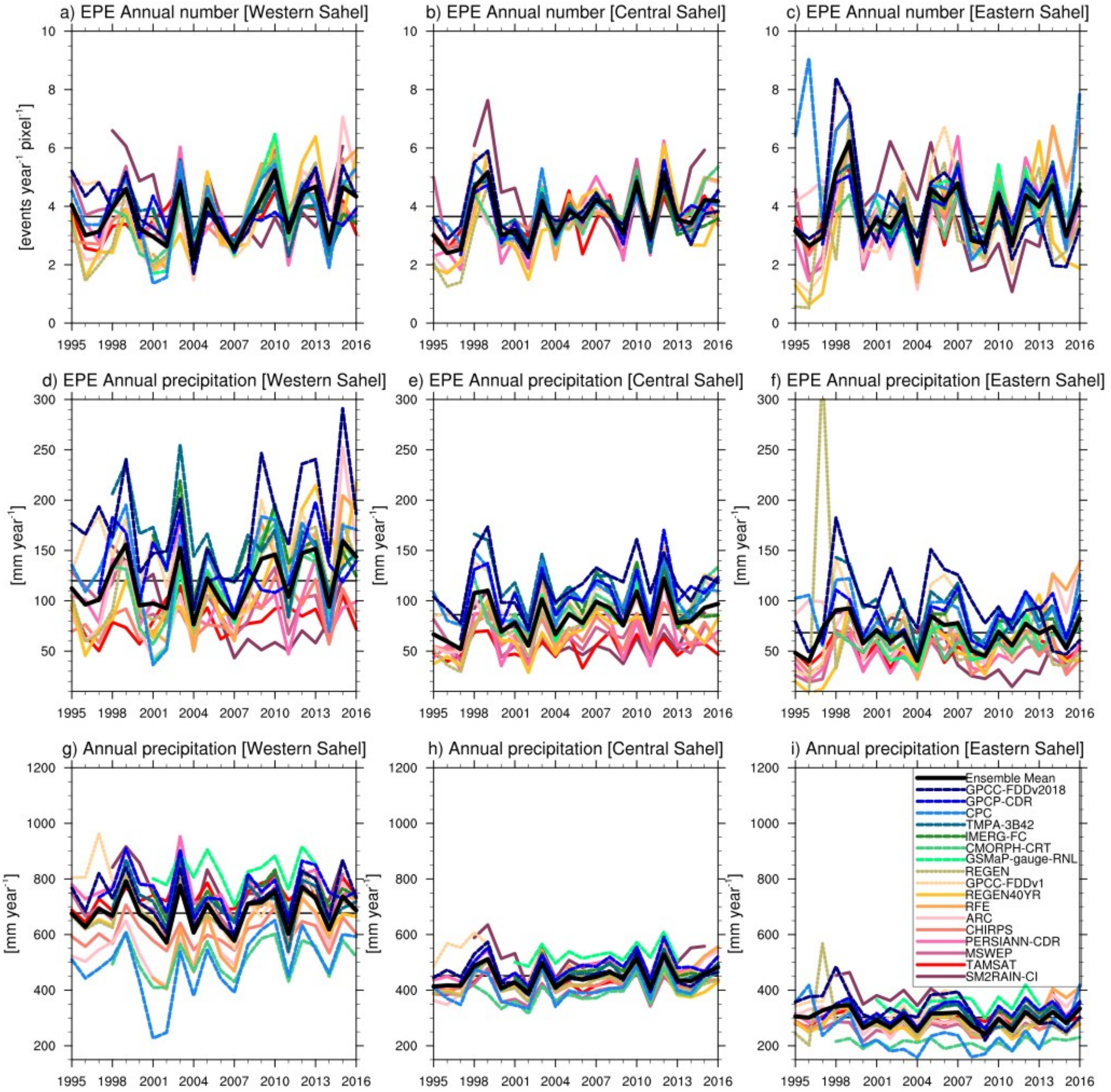

Figure 11: Same as Figure 10 but for (left) the Western Sahel, (middle) the Central Sahel and (right) the Eastern Sahel. The averaging domains are [10°N-20°N, 17°W-10°W], [10°N-20°N, 10°W-15°E] and [10°N:-20°N, 15°E-35°E], respectively.

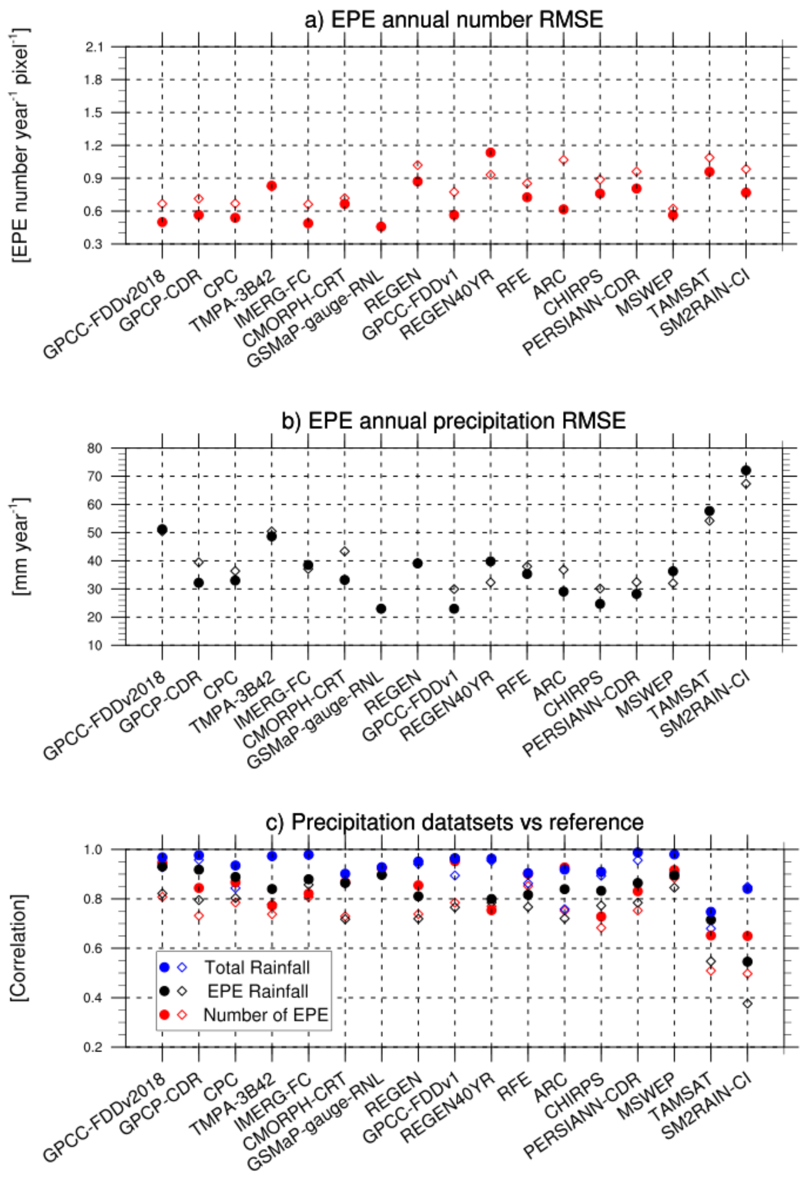

Figure 12: For each evaluated dataset, root mean square error (RMSE) of (a) the annual number of EPEs (events year^{-1} pixel^{-1}) and (b) the annual precipitation associated with EPEs (mm year^{-1}). (c) For each evaluated dataset, correlation between the total annual rainfall (blue symbols), the annual rainfall associated with EPEs (black symbols), the annual number of EPEs (red symbols), and their respective reference counterpart. RMSE and correlation are computed over time series averaged over the 15 pixels of Burkina Faso (i.e. time series of Figure 9). Dots indicate RMSE and correlations computed over 2001-2013, and open squares RMSE and correlations computed over the longest period common between the

corresponding dataset and the reference dataset. A linear trend was removed before computing the correlations. All correlations are statistically significant at the 95 % level using a two-sided t-test.

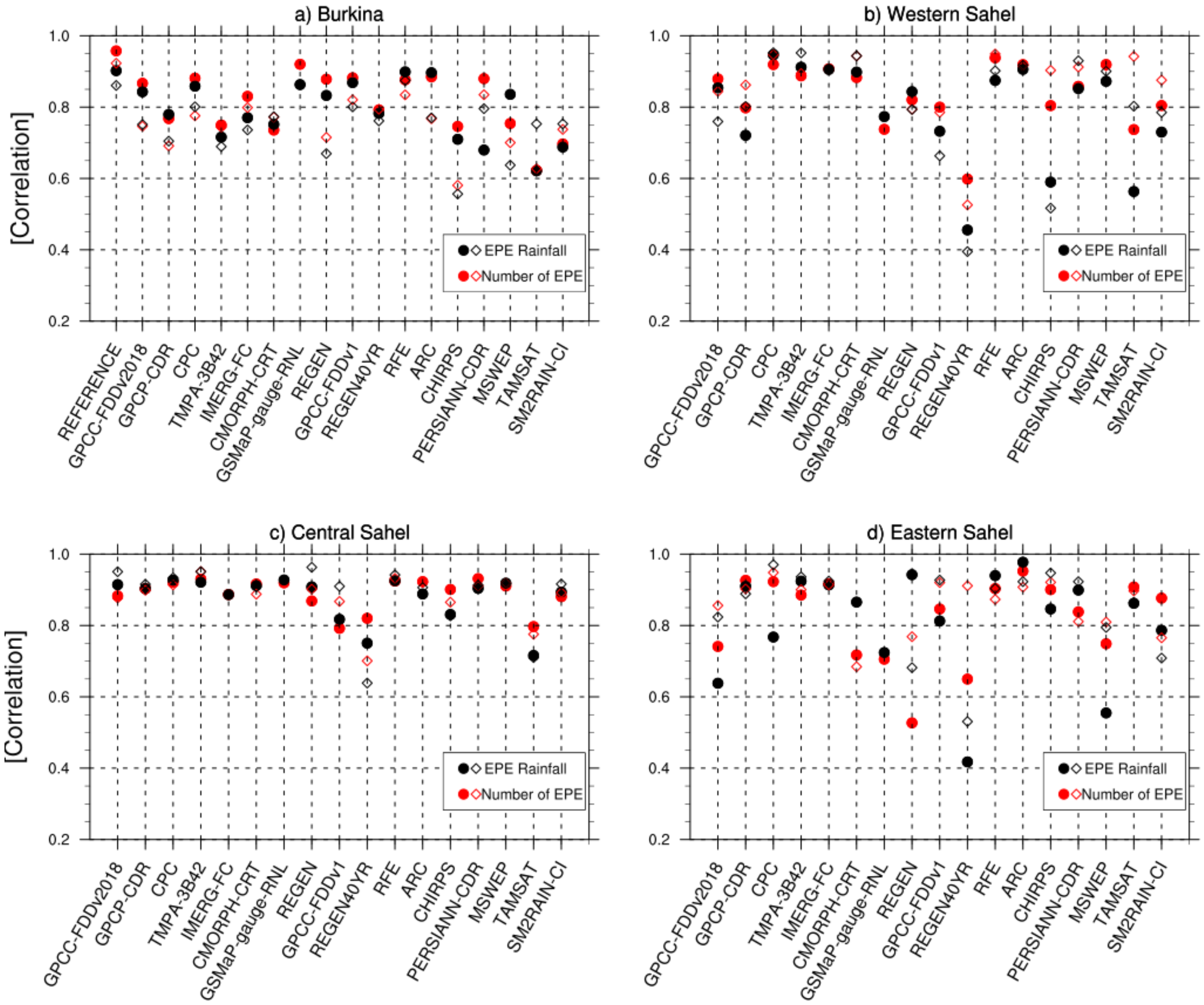

Figure 13: For each dataset, correlations between the annual total precipitation and EPE annual number (red symbols) or EPE annual rainfall (black symbols) for the average over (a) the 15 pixels of Burkina Faso, (b) the Western Sahel [10°N-20°N, 17°W-10°W], (c) the Central Sahel [10°N-20°N, 17°W-10°W] and (d) the Eastern Sahel [10°N-20°N, 15°E-35°E]. Correlations are computed over the time series shown in Figures 10 and 11. Dots indicate correlation computed over 2001-2013 and open squares correlations computed over the longest period common between the corresponding dataset and the reference datatset. A linear

trend was removed before computing the correlations. All correlations are statistically significant at the 95 % level a two-sided t-test.

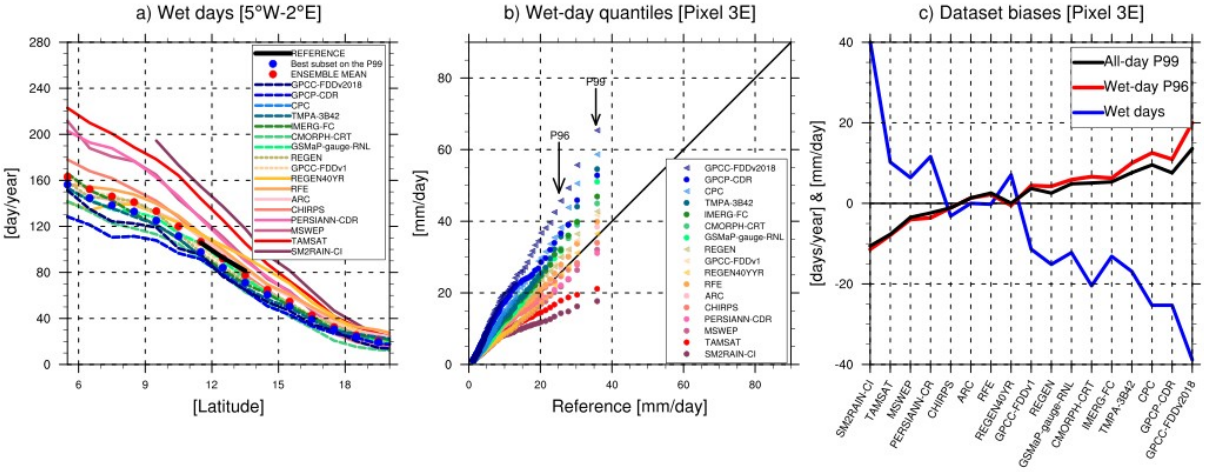

Figure 14: (a) Meridional profile of the mean annual number of wet days (day year^{-1}) averaged over the 5°W-2°E longitude band. (b) Same as Fig 2a but considering only wet days in the distribution of daily precipitation (precipitation above 1 mm day^{-1}). (c) For each evaluated P-dataset, bias of the all-day 99th percentile (mm day^{-1}, black line), the wet-day 96th percentile (mm day^{-1}, red line) and the annual number of wet days (day year^{-1}, blue line) with respect to the reference dataset. Only the pixel 3E is considered (Fig.1).

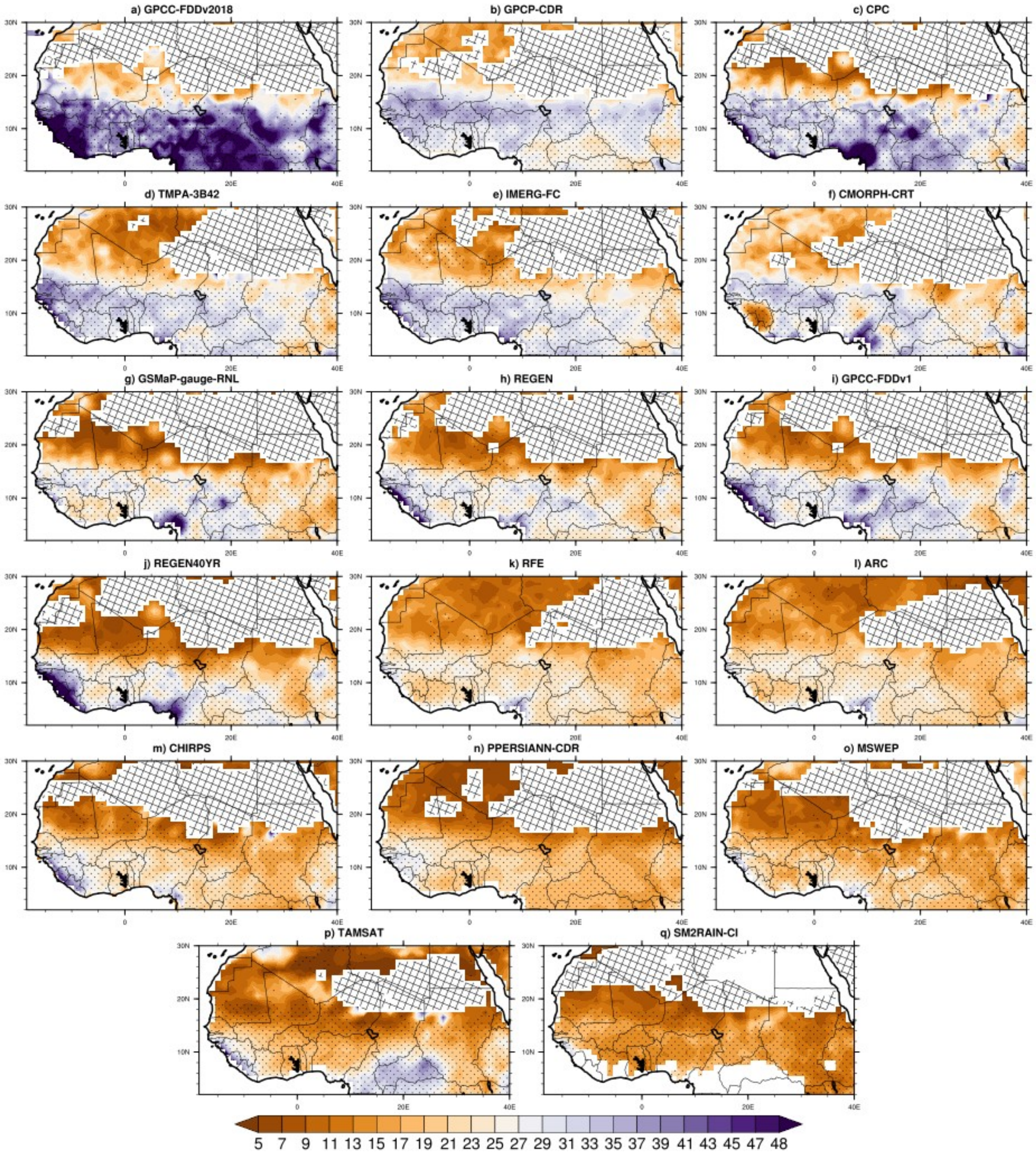

Figure 15: Same as Figure 3 but for the wet-day 96th percentile. Hatched pixels are the pixels where the percentile value is significant at the 95% level following a non-parametric bootstrap procedure and where its associated uncertainties is less than 15%.

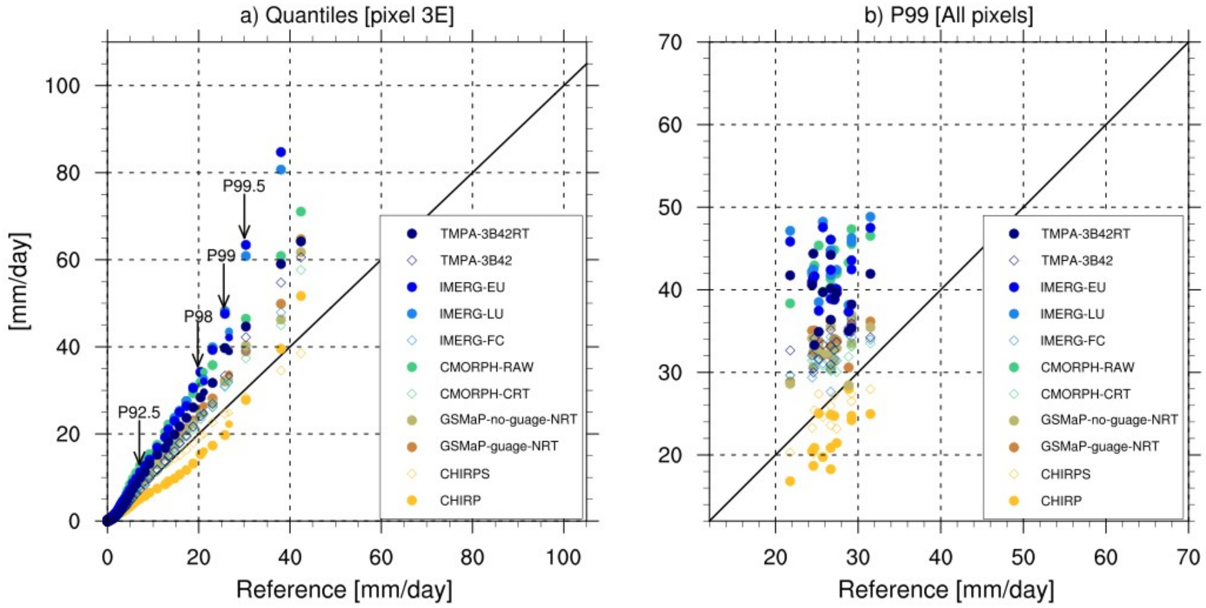

Figure 16: (a) and (b) Same as Figures 2a and 2b, respectively, but for the near-real-time P-datasets and their corresponding research products except that for GSMaP-gauge-NRT and GSMaP-no-gauge-NRT which is not analysed here.

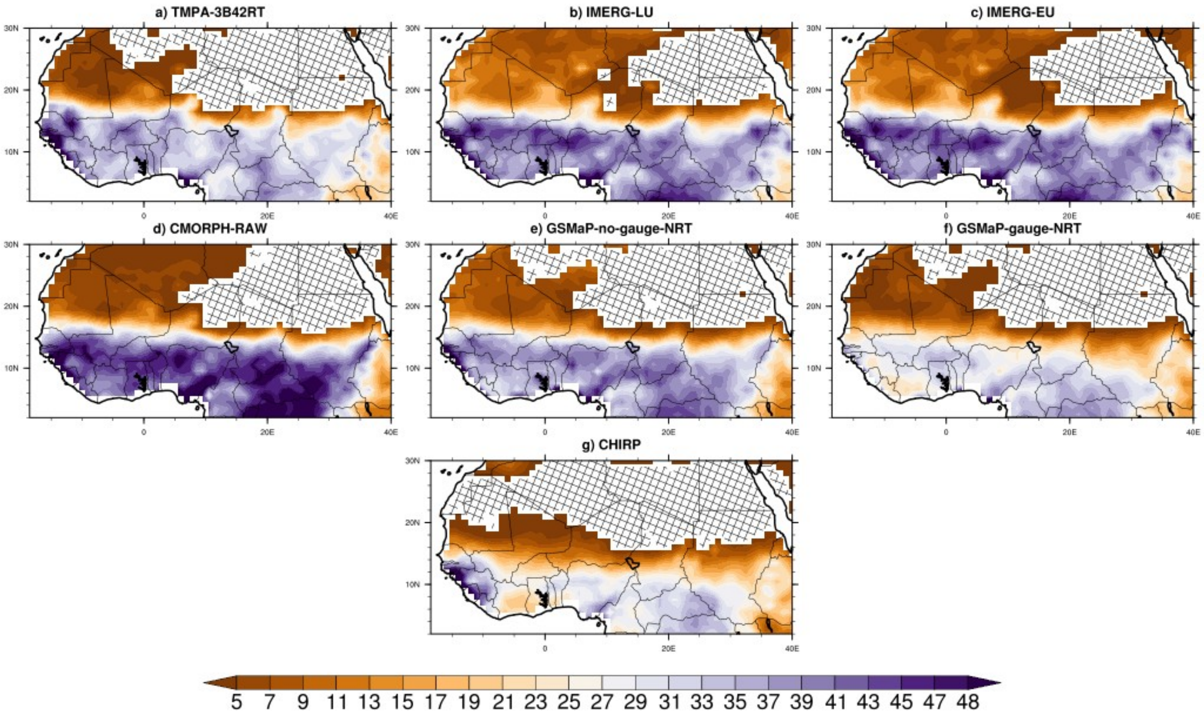

Figure 17: Same as Figure 3 but for the near-real-time products.